# Anti-lock Brake System Re-design and Control Prototyping using a One-Fifth Scale Vehicle Experimental Test-bed

**by**

**Chinmaya Baburao Patil, B.E.**

**THESIS**

Presented to the Faculty of the Graduate School of

The University of Texas at Austin

in Partial Fulfillment

of the Requirements

for the Degree of

**MASTER OF SCIENCE IN ENGINEERING**

THE UNIVERSITY OF TEXAS AT AUSTIN

August 2003

**Anti-lock Brake System Re-design and Control Prototyping using a One-Fifth Scale Vehicle Experimental Test-bed**

APPROVED BY

SUPERVISING COMMITTEE:

Raul G. Longoria, Supervisor

Richard H. Crawford

To my dear parents.

# Acknowledgments

As with most works of any significance, this thesis has been accomplished with the direct and indirect contributions from a number of people.

First and foremost, I would like to express my sincere gratitude to my supervisor, Dr. Longoria, for his sustained encouragement and enthusiasm throughout the duration of the project. His support at the outset of the project is gratefully acknowledged.

I would like to gratefully acknowledge the support from National Instruments for the project. Sincere thanks go to Ravi Marawar, Sugato Deb, John Limroth and Joseph Hays, for their numerous ideas and suggestions, and most importantly, patience and understanding all along the course of the project.

I wish to thank Dr. Crawford for his time in reading the thesis and offering useful suggestions.

Sincere gratitude is extended to fellow members of the 'System Modeling and Experimentation' group, in particular, Fu Zhang, Gilberto Lopez, Chayawee Wangcharoenrung and Kim Seyoon, for all the help and co-operation. Thanks go to Charles Webber, for helping with shop work.

I wish to acknowledge the efforts of Amrou Adly Al-Sharif in setting up the Scaled Vehicle Laboratory, which formed the groundwork for this thesis. Thanks go to Anish Mathews for suggestions regarding usage of LabVIEW.

All my friends, old and new, and the list is long, in Austin and the

United States, need special mention for making living here, homely and fun.

Lastly, to my parents, without whose faith, support and love, this work would not have been possible, I extend my utmost respect and gratitude.

# Anti-lock Brake System Re-design and Control Prototyping using a One-Fifth Scale Vehicle Experimental Test-bed

Chinmaya Baburao Patil, M.S.E.
The University of Texas at Austin, 2003

Supervisor: Raul G. Longoria

This thesis documents the efforts to examine the rapid control prototyping of an antilock brake system (ABS) using a one-fifth scaled vehicle test-bed. The brake system on the scaled test vehicle is modeled using a frequency response approach, to facilitate experimental system identification and control design. Dynamic performance of the brake system is improved by suitably redesigning the components to subdue the effects of the patent static nonlinearities, and using a phase-lead compensator in closed-loop operation. Two control schemes, namely, the bang-bang control and the sliding mode control, are formulated for ABS and the designs are fine-tuned by simulations. Hardware-in-the-loop testing of these control schemes with the scaled vehicle setup is conducted for three panic braking scenarios, and a comparison of their performance based on improvement in stopping distance is presented. Dimensional analysis allows the control schemes to be re-written using dimensionless terms for extrapolation to a full-sized vehicle.

# Table of Contents

# List of Tables

# List of Figures

# Chapter 1

# Introduction

Rapid control prototyping is a very popular technique for testing control system prototypes on the actual physical hardware or the plant before final implementation. Evaluating the performance of the control system in the real-world environment (where it will eventually operate), while still in the controller design process, provides critical information regarding both the system and the controller. As the control algorithm is implemented in software, changes to the design can be accomplished quickly, thereby reducing the overall design cycle time of the control system. The efficient implementation of the technique is promoted by the advances in real-time computing hardware and software and better integration of simulation and testing tools. The technique is extensively applied in the automotive industry, as automobiles are becoming increasingly 'intelligent'. Complex control algorithms are employed to control critical functions, like engine management, vehicle safety, performance handling, etc., all of which serve to provide a better ride to the passengers. Automotive engineers are resorting to rapid control prototyping method to realize these control schemes quickly and efficiently. In this thesis, the application of rapid control prototyping method for the design of antilock brake system is investigated.

With an astronomic increase in road traffic around the world, on-road vehicular safety has assumed enormous importance. Traffic regulatory author-

ities in many countries have made it mandatory for auto makers to include several critical safety systems in vehicles. Antilock Brake System (ABS) is among the most important safety systems in a vehicle. It prevents tire lock-up under critical braking conditions, such as those encountered with wet or slippery road surfaces, driver panic reaction (unanticipated obstacle) etc., [3]. Tire lock-up has many deleterious effects on vehicle safety, namely, loss of directional stability, increase in vehicle stopping distance (in most cases), jack-knifing in trailers and so on. By preventing tire lock-up ABS ensures that the vehicle remains responsive to steering wheel inputs. Reduced stopping distance on account of ABS is more evident on wet or slippery road surfaces [12]. The National Highway Traffic Safety Administration (NHTSA) requires through regulations FMVSS 121 (for 'Air Brake Systems') and FMVSS 105 (for 'Hydraulic Brake Systems') that ABS be installed on all commercial vehicles (with gross vehicle weight ratings of more than 10,000 lbs) built on or after March 1, 1998, for air-braked vehicles and March 1, 1999, for hydraulically braked vehicles. However, even though the Agency does not require ABS on light vehicles (gross vehicle weight rating (GVWR) of 10,000 pounds or less), light vehicle manufacturers are currently voluntarily equipping a large percentage (approximately 55 percent) of new light vehicles with ABS [22].

ABS is a closed loop control system which modulates the brake torque that is applied to the tires depending upon the state the tires are in, to prevent them from locking up. The other important function of the ABS is to exploit the maximum traction available from the road surface. The tire-road surface interaction is essentially nonlinear in nature and exhibits tremendous variability depending upon the tire tread characteristics, tire inflation pressure, vertical load on the tire, vehicle speed, the road surface, presence of water or

other extraneous matter at the interface and so on [4]. This makes the task of developing control schemes for ABS a very challenging one and the problem is very popular in the field of vehicle dynamics research. Many control schemes have been designed including nonlinear PID [5], sliding mode control [6] [7] [8], adaptive control [9], neural network approach [10], fuzzy logic control [11] etc. The design of these control systems is very often an iterative process and they require extensive testing before the actual implementation. This prompts the use of rapid control prototyping method for their design. However, testing with real full-sized vehicles is a very time and cost intensive process and iterating through different test cases slows down the entire control prototyping cycle. Scaled systems provide a turnkey solution to this problem.

Dynamically similar fractional scale systems have been used in place of actual systems by exploiting similitude principles to obtain valuable information about them via testing. They enable the test engineer to quickly test the system for many what-if conditions. Active research is on to investigate using fractional scale vehicles for vehicle dynamics study and also as a platform for rapid control prototyping. Brennan and Alleyne [13] describe using scaled vehicles for steady state lateral vehicle dynamics study. J. Sika et al [14] use a scaled vehicle to study lateral control of a vehicle in an automated highway system. Kachroo and Özbay [15] employ a similar approach to the study of automated highway systems using scaled vehicles. Scaled vehicles are particularly well suited for ABS control testing as full size vehicle testing is potentially hazardous for the driver and the vehicle. Cuderman [16] describes an ABS testing procedure with full size vehicles and the necessary safety precautions for the driver. With scaled vehicles extreme conditions can be quickly and safely simulated and the control prototyping process can be effectively expedited.

In addition, a scaled system provides an effective educational environment for advanced vehicle controls studies.

This thesis looks at using a scaled vehicle setup previously built [1] for designing and implementing two different control schemes, namely, bang-bang control and sliding mode control, for ABS. Al Sharief [1] describes conventional braking and antilock braking with bang bang control. Mathews [2] explores fuzzy control for ABS with adaptability to different road surfaces. Test results from both works indicate unsatisfactory antilock braking performance. The current work investigates the causes and addresses the issue by carrying out the redesign of the actuator system to improve its performance. The brake system is modeled parametrically and the model is fine-tuned using frequency response data. The model is used to identify the static non-linearities which are then eliminated or minimized by redesiging the components responsible. Compensators are then designed based on the redesigned brake system model to improve the braking performance. Control prototyping is then carried out and the performance of the brake system is evaluated by hardware-in-the-loop testing with the brake system as physical hardware.

The thesis is organized as follows: Chapter 2 covers a brief overview of the scaled vehicle laboratory and a description of the control prototyping procedure that is used in the current work. Chapter 3 contains the details of the scaled vehicle brake system modeling and the redesign efforts. Chapter 4 looks at the problem of ABS control and investigates the design and implementation of two control schemes for ABS on the scaled vehicle. The test results are provided along with a discussion of the actuator performance in the two control schemes. Chapter 5 includes the summary of the thesis and the concluding discussion and suggestions for future work. All the parameters

pertaining to the scaled vehicle, the brake system and the surface properties are listed in Appendix A. A discussion of the ABS test procedure with the scaled vehicle is discussed in Appendix B.

# Chapter 2

# Scaled Vehicle Laboratory Setup

This chapter discusses the scaled vehicle laboratory setup employed for ABS control prototyping in this work. An overview of the setup is given first and then the control prototyping process is described in context of the setup. A detailed description of the laboratory setup can be found in [1]. A few modifications have been made to the original setup design and they have been emphasized in the following discussion.

## 2.1 Scaled Vehicle Setup

The Scaled Vehicle Laboratory was built with the objective of being able to study vehicle dynamics, explore the implementation of various active vehicle control systems and evaluate different algorithms as well as the hardware used for vehicle control by testing [1]. Scaled vehicles provide a convenient platform to quickly implement different control schemes for various active vehicle systems like ABS, lateral control, suspensions, traction control, etc., and for evaluating their performance by testing. They provide the system design engineer the flexibility to study the physical system's behavior under simulated extreme test conditions which may be difficult to reproduce in simulation environments and potentially hazardous for full sized vehicle testing. The prime benefit of using scaled vehicles, however, lies in the substantive reduction in the cost, time and effort involved in testing, which implies that

several test iterations can be carried out in the time period needed for a single full sized vehicle test. This renders scaled vehicles very attractive for the control prototyping process which is inherently iterative in nature.

### Test Vehicle

The laboratory setup used in this work revolves around a one-fifth scale test vehicle (referred to as 'test vehicle' henceforth). This Porsche GT2 replica model, made by FG Modellsport, is equipped with a gas-powered IC engine with single speed rear-wheel drivetrain, servo-motor actuated disk brakes on the front wheel and four wheel independent wish-bone suspension system. The throttle and Ackermann steering are also servo-actuated and are operated manually by radio control or are controlled by an on-board microprocessor for cruise control and ABS implementation. Fig. 2.1 shows a picture of the test vehicle. The test vehicle has 'bald' tires so effects of the tire treads on any form of traction testing are not accounted for, and the problem of tire wear is overcome. Structural modifications have been made to the test vehicle to expand the testing capabilities. The brake system has been modified so that each of the front wheels can be individually braked. A more detailed description of the brake system is given in Chapter 3. Optical sensors have been mounted on the two front wheels and the rear differential to provide wheel and vehicle speed data. A triaxial accelerometer provides longitudinal and lateral acceleration data. The power supply and signal processing/amplification for all the sensors and actuators on the vehicle is centrally handled by an on board transfer box. Numerical values of relevant test vehicle parameters are given in Appendix A.1.


Figure 2.1: Test Vehicle [19].

**Test Equipment**

The microprocessor controller has been replaced by a stand-alone National Instruments PXI real-time Embedded Controller module. The real-time controller runs LabVIEW RT which facilitates implementation of control algorithms in the test environment of LabVIEW, enabling quick and easy testing. The embedded controller communicates over TCP/IP with a host PC. The host is used to design control schemes and transform the algorithms into 'code' suitable for execution on the embedded controller in real-time. The

data acquisition unit for the controller comprises of a multi-purpose NI PXI 6070E data acquisition card and an NI 6602 counter/timer card, which running synchronously provide 16 single-ended analog input, 2 analog output (12-bit resolution), 8 digital I/O channels along with 8 32-bit counters. A shielded cable forms a communication bus between the data acquisition unit and the transfer box on the vehicle, carrying actuator control signals and sensor data, besides two levels of power supply (+5V, 1A and ± 15V, 0.3A) from a dedicated source. This configuration provides the laboratory setup the flexibility of augmenting the vehicle with additional sensors/actuators so that it can be employed to investigate many vehicle control systems like active suspension system, steering control, and so on, apart from ABS control.

**Test Area**

The testing area, designed specifically for ABS testing, consists of a curvilinear accelerating ramp and a test track. A picture of the testing area is shown in Fig. 2.2. A winch motor is used to hitch the test vehicle up the ramp to a predetermined height. The ramp merges with the track in a smooth circular arc thus ensuring a jerk-free transition of the velocity from the accelerating phase to the braking phase[1]. The test track can be overlaid with different synthetic surfaces to emulate different road surface conditions. The laboratory currently uses three surfaces which simulate the differences that would be seen between icy, wet and normal (dry) road conditions.

[1]See Appendix B.

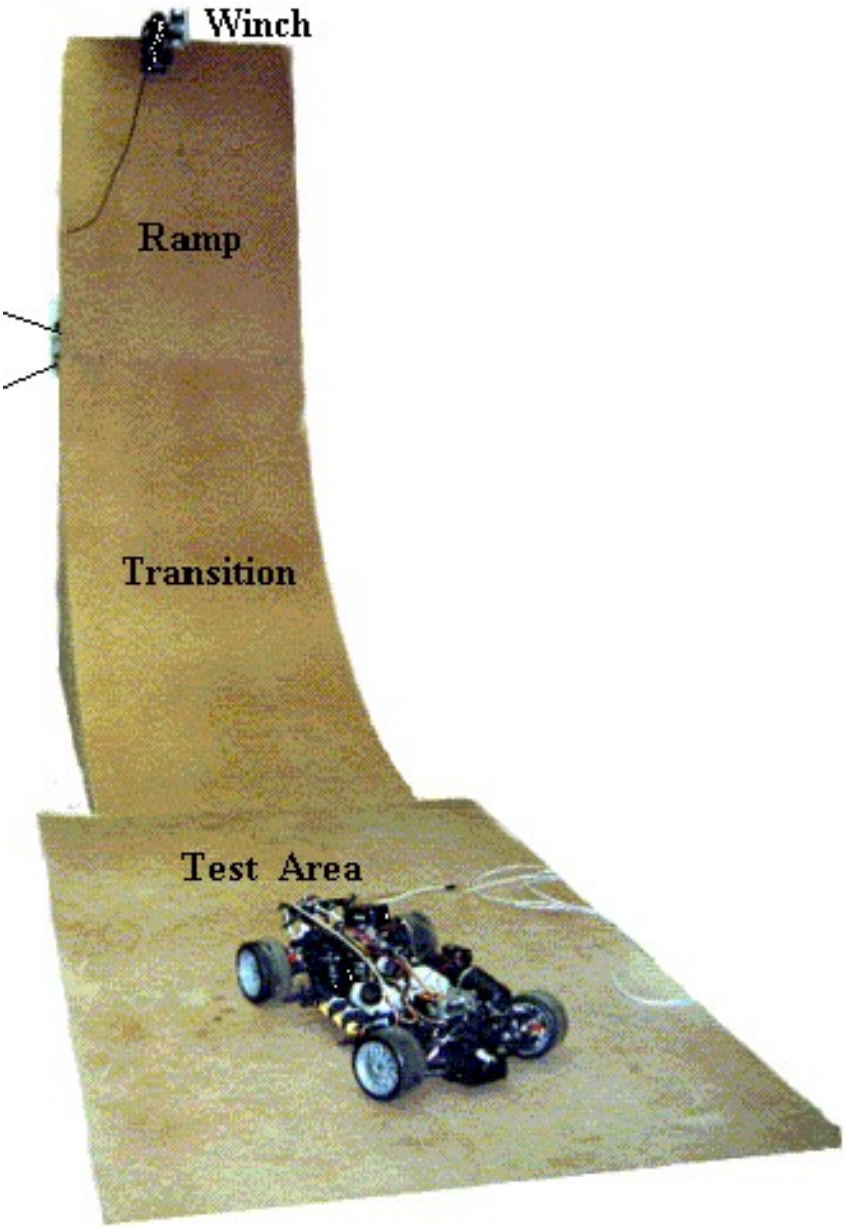


Figure 2.2: Test Area for Scaled Vehicle ABS Testing.

## 2.2 Rapid Control Prototyping

Rapid control prototyping is a method for evaluating the performance of a control system by implementing it in software and testing it with the physical system (software-in-the-loop testing). Modern control systems, designed to be optimal in performance with respect to some specified criterion, robust to changes in system and environmental parameters and in some cases adaptive in operation, are usually complex in their structure and require extensive simulation and testing before final implementation. By quickly implementing them in software (in the form of code generated from the simulation model) and investigating their operation with physical systems, their effectiveness in real world operating conditions can be studied up front and trade-off decisions relating to their design can be made more judiciously [17]. The process can also be employed to guide the design and selection of actuator and sensor subsystems thus facilitating integrated development of the mechatronic control systems. Rapid control prototyping is playing a central role in the development of various vehicle control systems as they are predominantly mechatronic in nature [18].

Real-time implementation of the control scheme becomes necessary for testing with the actual physical system. The advancements in hardware technology capable of 'hard' real-time computation and seamless integration of simulation and testing software has greatly benefited the prototyping process. Many software tools are commercially available for control prototyping implementation, some being generic control systems design tools like LabVIEW RT, MATLAB/Simulink/Realtime Workshop etc., while some are solely dedicated like dSPACE, Opal-RT, etc. Central to these tools is the ability to generate code from simulation models which can run in real-time and the necessary

hardware to run the code and test it with physical systems.

Fig. 2.3 shows what could be a typical iterative control system design process with all the salient stages. The details of the control prototyping process that will be followed in this work are shown in Fig. 2.4. Once a control system is designed using the MATLAB/Simulink[2] simulation tool on the host PC to obtain satisfactory performance, the Simulink Realtime Workshop is used in conjunction with the LabVIEW RT Simulation Interface Toolkit[3] to generate a LabVIEW program, a Virtual Instrument (VI), for execution on a real-time embedded controller. The real time module communicates with a host PC via a TCP/IP network, using the National Instruments' VI Server technology. The VI is downloaded and executed on the embedded controller module. LabVIEW RT generates two processes, one on the embedded controller and the other on the host machine, both of which run concurrently. The host-side process handles the user interface; the embedded portion runs the control loop. The two machines exchange information and permit changing control parameters during execution of the program. The execution on the embedded controller is independent of the host machine. In the absence of communication from the host, the embedded program continues to operate with current parameters autonomously. This is essentially the same scenario as the deployment of the production code, so the transition from design to implementation is smooth.

[2]The MathWorks Inc.,
[3]National Instruments

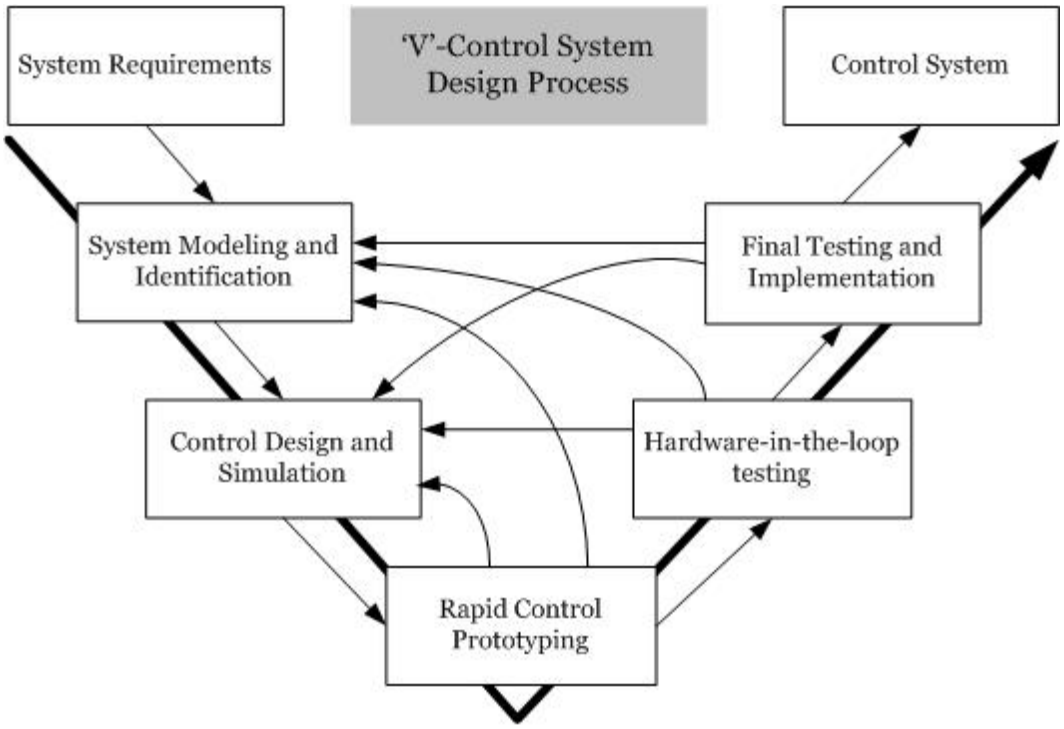


Figure 2.3: Schematic of a typical Control System Design process.

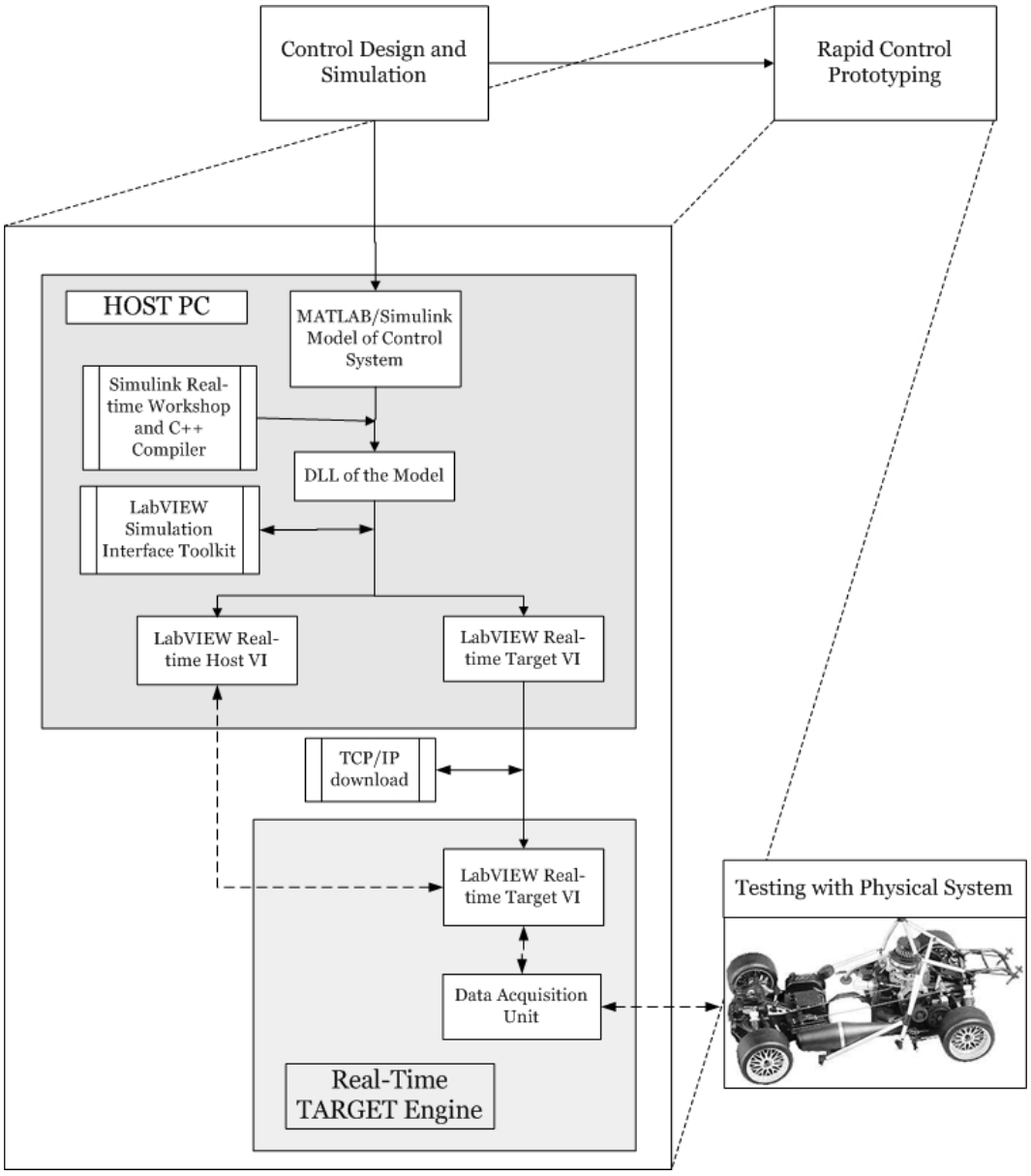


Figure 2.4: Schematic of a typical control prototyping process, implemented with current software and hardware tools.

# Chapter 3

# Brake System Modeling and Re-design

This chapter discusses the scaled vehicle brake system characterization and the redesign efforts directed at improving the performance of the system. The requirements of an antilock brake system for the scaled test vehicle are described first, comparing them with that of full sized vehicles. A brief description of the electromechanical brake system on the test vehicle is then introduced and a parametric bond graph model is developed for the same. The model is fine tuned using experimental frequency response data and the brake system performance is evaluated against the criteria previously established. Redesign tasks to improve the dynamic response of the system are identified and implemented. A transfer function model is then developed for the redesigned brake system via frequency response studies. The model is for the design of compensators to further increase the system bandwidth. The improvement in the redesigned system performance is evaluated in Chapter 4 via testing the ABS action with two different control schemes.

## 3.1 Antilock Brake System Requirements

The dynamics of braking of a generic vehicle help to define the requirements for an antilock brake system, and to idenfity two critical factors: the maximum brake torque and the system bandwidth. Fig. 3.1 shows one wheel of a vehicle (i.e., a 'quarter-car' model) subjected to brake torque, $\tau_{brake}$, with

all the forces acting on it. Here, $W_{tire}$ is the normal load on the tire, expressed as some fraction, $K$, of the vehicle weight $W$, $F_r$ is the braking force on the vehicle from the road surface, $V$ is the vehicle speed, $\omega$ is the wheel angular velocity and $R_{tire}$ is the tire radius. The equations of motion of the tire under

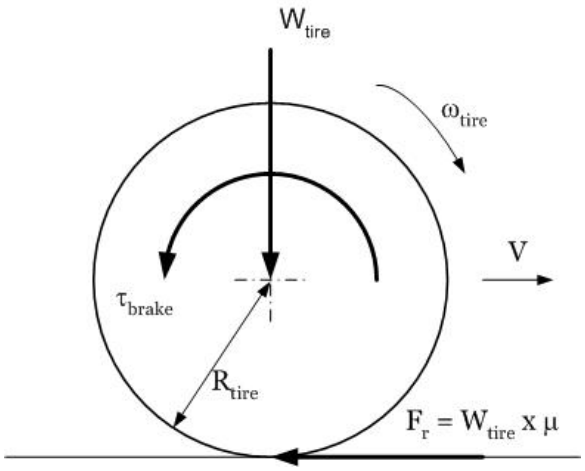


Figure 3.1: Quarter-car Braking Model.

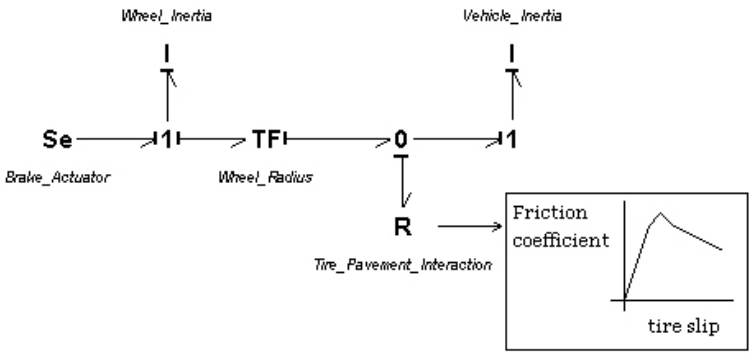


Figure 3.2: Bond Graph representation of the Quarter-Car Model.

braking can be formulated from the bond graph representation of the model,

shown in Fig. 3.2, and are

$$\begin{aligned} \frac{W}{g} \cdot \dot{V} &= -n \cdot F_r \\ \Rightarrow \dot{V} &= -n \cdot K \cdot g \cdot \mu \\ J_{tire} \cdot \dot{\omega} &= F_r \cdot R_{tire} - \tau_{brake} \\ \Rightarrow \dot{\omega} &= \frac{1}{J_{tire}} \cdot (K \cdot W \cdot R_{tire} \cdot \mu - \tau_{brake}), \end{aligned} \tag{3.1}$$

where, $n$ corresponds to the number of wheels subjected to braking and $J_{tire}$ is the tire rotational inertia.

The objective of this vehicle braking system is to stop the vehicle in the shortest possible distance, ideally, which translates into achieving maximum deceleration. From the $\dot{V}$ equations in (3.1), we see that, for a given vehicle, this amounts to maximizing $\mu$, the friction coefficient at the tire-road surface interface. By virtue of the fact that $\mu$ is a function of the tire slip $\lambda$ (see Chapter 4), the tire dynamics given by the $\dot{\omega}$ equation in (3.1) governs the response of the tire and hence that of the vehicle to the braking action. From the bond graph we see that the tire inertia $J_{tire}$ and the tire-road surface interaction are analogous to a first order rotational mass-damper system. From linear system theory, an approximation for the system 'time constant' can be extracted from the $\dot{\omega}$ equation as,

$$\mathcal{T} \approx 2\pi \cdot \left( \frac{J_{tire}}{K \cdot W \cdot R_{tire} \cdot \mu_{avg}} \right)$$

where, $\mu_{avg}$ is the average value of the friction coefficient determined over the time period of braking 'T'. The '$2\pi$' term is used for dimensional homogeneity. The system's response bandwidth is calculated as the reciprocal of the time constant.

For a typical vehicle, with mass = 1000kg, tire radius $R_{tire} = 0.33m$, $K$= 0.5*40%, tire rotational inertia $J_{tire} \approx mR_{tire}^2 = 40 * (0.33)^2\ kg - m^2$ and $\mu_{avg} \approx 0.9$ for braking on dry road surface, the system bandwidth equals $21Hz$. This is the frequency at which most commercial ABS operate [3]. For the scaled test vehicle, with the corresponding parameter values of: mass= $9kg$, tire radius $R_{tire} = 0.061m$, $K = 0.5$*41%, $J_{tire} = 9.678$e-4 $kg$-$m^2$ and $\mu_{avg} \approx 0.75$, the system bandwidth approximately equals $136Hz$. The high speed of response of the scaled vehicle to braking action is explained by the small rotational inertia of the tire. While this is an approximation, it does give a range wherein the brake actuator bandwidth must lie for 'perfect' antilock braking operation (i.e., perfectly maintaining the slip at a desired value), thereby maximizing the vehicle deceleration.

The actuator capability in terms of the maximum brake torque can also be obtained from equation (3.1). Writing $\dot{\omega}$ as $\alpha$, the brake actuator must be able to apply a maximum torque equal to,

$$\tau_{brake:max} = J_{tire} \cdot |\alpha_{des}| + K \cdot W \cdot R_{tire} \cdot \mu,$$

where $\alpha_{des}$ is the desired tire deceleration which must exceed $\left|\frac{\dot{V}_{max}}{R_{tire}}\right|$, or,

$$\tau_{brake:max} > \frac{1}{R_{tire}} \cdot J_{tire} \cdot n \cdot K \cdot g \cdot \mu_{max} + K \cdot W \cdot R_{tire} \cdot \mu_{max}. \qquad (3.2)$$

For the scaled vehicle this translates into $\tau_{brake:max} > 1.145 \cdot \mu_{max}$, where $\mu_{max}$ is the peak friction coefficient offered by the tire-road surface interaction. The larger the brake torque capacity of the actuator, the greater the tire deceleration, but greater is the demand on the dynamic performance of the actuator.

In the next section the electromechanical brake system on the test vehicle is described and its performance is evaluated via modeling.

## 3.2 Brake System Modeling

The scaled test vehicle has an independent front tire floating caliper-disk brake system, actuated by DC motors. The DC motors are actually Futuba servo-motors with their feedback circuits removed. By using the servos as simple DC motors, greater flexibility in control is ensured while still using their compact reduction gear train to increase output torque capability. The DC motors are driven by a power amplifier operating in a transconductance circuit configuration, which makes it possible to implement current-control of the motors. A cable transmits the motor torque to a lever and cam mechanism which provides mechanical advantage to amplify the motor torque being applied to the brake calipers. Fig. 3.3 shows the picture of the brake system.

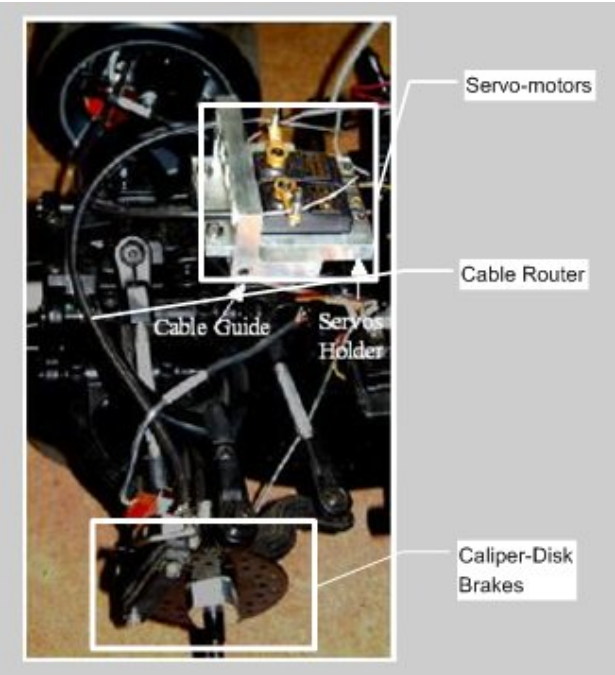


Figure 3.3: Electromechanical Brake System on the Test Vehicle.

### 3.2.1 Parametric Modeling

A bond graph model (with the state equations) of the brake system would help to understand the structure of the system and focus the redesign efforts on specific components which can be identified as the cause of the subpar performance. Fig. 3.4 shows a schematic representation of the system, which can be used to develop a detailed bond graph model for the system, as shown in Fig. 3.5 (see Appendix A.2 for description of the parameters). The model can be simplified by analytically lumping the dependent energy storage elements with independent ones and disregarding the contribution from components with high speed of response in favor to that from slower responding ones.

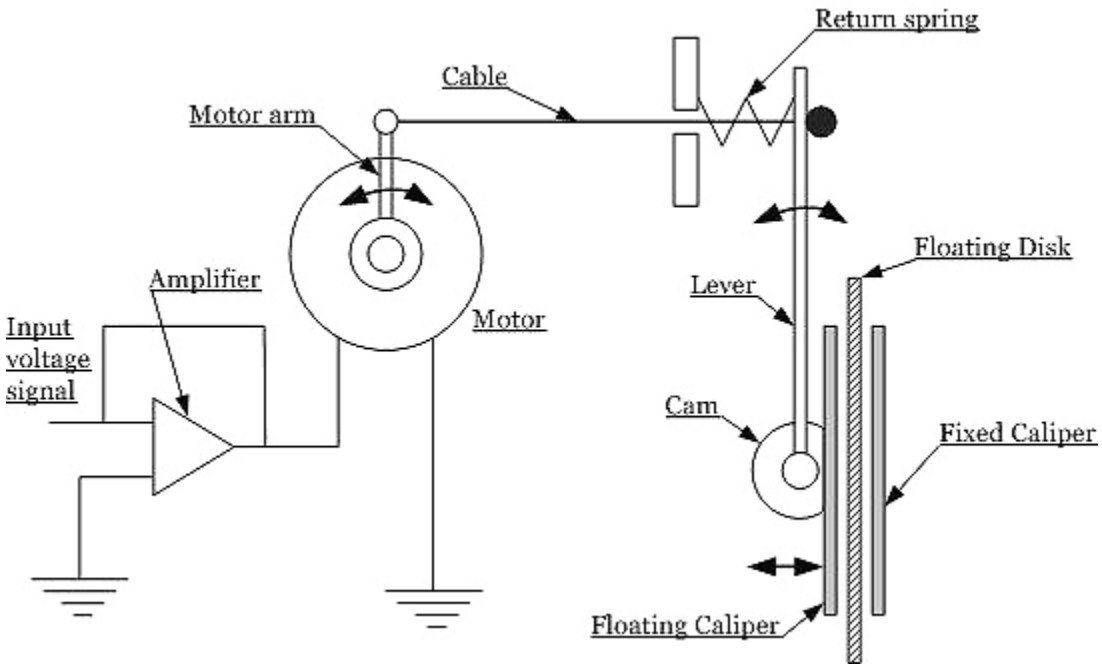


Figure 3.4: Schematic representation of the Electromechanical Brake System.

However, two factors qualify the fidelity of such a parametric model, namely,

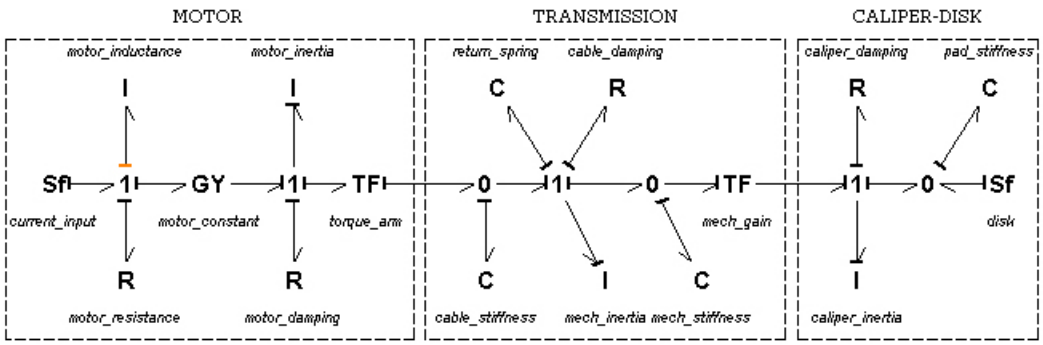


Figure 3.5: Bond Graph representation of the Electromechanical Brake System.

1. the lack of complete parametric data for the brake system.

   Efforts were made to characterize the different components of the system. As the scale of operation is small, the numerical accuracy of the measured parameters has to be significantly high. Since it was difficult to maintain the level of accuracy in measuring parameters of some of the components, for example, the stiffness of the brake pads, the characterization experiments were discontinued.

2. the presence of significant non-linearities in the system which affect its performance.

   Fig. 3.6 shows results of testing bang-bang ABS control with the brake system. The 'control input' is the voltage signal applied to the servo actuators to apply the brakes. The system response shows considerable time-lag, which is a clear indicator of the presence of static nonlinearities in the system. Analytical characterization of the nonlinearities would make parametric modeling very tedious and the outcome would still be

only an approximation of the actual system.

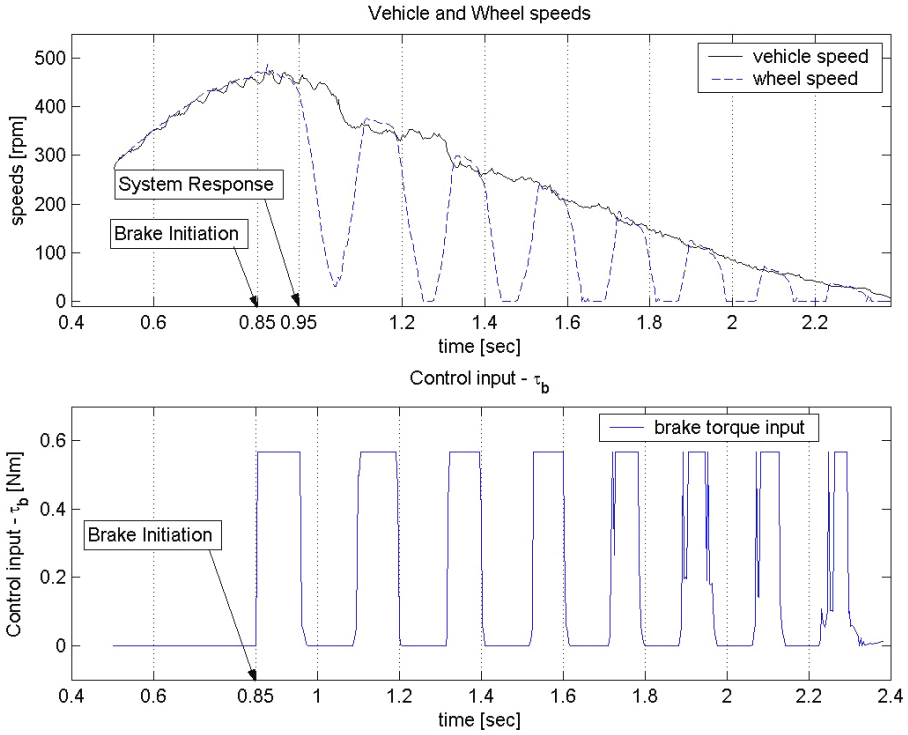


Figure 3.6: Bang-bang ABS Control Test Result (before re-design).

An alternative and a more convenient approach is to characterize the brake system experimentally and develop an input-output transfer function model that represents the entire system. The system transfer function is equivalent to a state-space model, except that the physical interpretation of the phase variables that represent the states is difficult. Though this would preclude full state feedback control by measurement, state observers can be used to obtain the values of the phase variables. In this work, however, the

transfer function will be used for simple dynamic compensator design. This is discussed in the next section.

### 3.2.2 Frequency Response Modeling

Identification of the brake system model via frequency response data addresses both the concerns of parametric modeling mentioned above. By treating the brake system as a black box and measuring the response characteristics namely, the magnitude and phase-shift, to sinusoidal inputs of varying frequency, we can generate a 'Bode' plot representing the system's open-loop behavior. The system order and corner frequencies can then be determined from the asymptotic approximations to the Bode plots by trial-and-error [17] to give the system transfer function. The range of input signal frequency must be large enough to cover the system's operating range. A requirement for the frequency response method to work is that the system under consideration must be linear, so that for a sinusoidal input, the output is also a sinusoid of the same frequency. As the brake system on the scaled vehicle was shown to possess nonlinearities, the frequency response experiment can be used to identify and estimate their extent. If the system has dynamic nonlinearities, like algebraic, transcendental, exponential etc., the frequency of the output will not be the same as that of the input. However, if the nonlinearities are static like deadband, hysteresis, saturation, the fundamental output harmonic frequency and the input frequency match, but the output is not sinusoidal in nature. In the latter case, the static nonlinearities can be approximated by suitable 'describing functions' by neglecting their higher harmonics and a linear approximation model can be developed for the system.

As shown in the bond graph, the input and the output for the brake

system are the current from the amplifier (or the voltage signal to the amplifier) and the force on the disk (or the brake torque) respectively. A test setup was built to conduct the frequency response study with the input signal being generated by a function generator LabVIEW VI running on the real-time embedded controller and the output force being measured by a load cell. A biased sinusoidal drive signal was used since the output force is always positive semi-definite, and it would not respond to the negative going portion of an unbiased sine wave. The response of nonlinear systems is not only dependent upon the frequency of the input but also on the amplitude. This requires testing the system over a range of input amplitudes as well as sweeping the frequency. However, it was observed that until the input voltage reached a threshold value of $2V$ peak-to-peak no force was measured at the brake calipers and beyond that the amplitude of the force output was proportional to the input voltage amplitude. Therefore a complete input frequency sweep was carried out only for one value of amplitude and bias. The frequency was swept starting from a low value of $0.2Hz$, in steps of $0.2Hz$, up to $10Hz$, beyond which the signal-to-noise ratio diminished rapidly. The setup to carry out the swept-sine testing on the brake system is shown in Fig. 3.7.

The output force from the frequency response tests for two particular inputs of frequencies, $3Hz$ and $8Hz$, are shown in Fig. 3.8. The test results depict only a small window of the entire test period which was consistent across two iterations. As seen in the two input-output plots, although the output is not sinusoidal in nature, the fundamental harmonic frequency does match that of the input. This observation indicates that the significant nonlinearities in the system are static in nature. The bode plot of the system, with the voltage signal to the amplifiers as the input and the force at the brake calipers as the

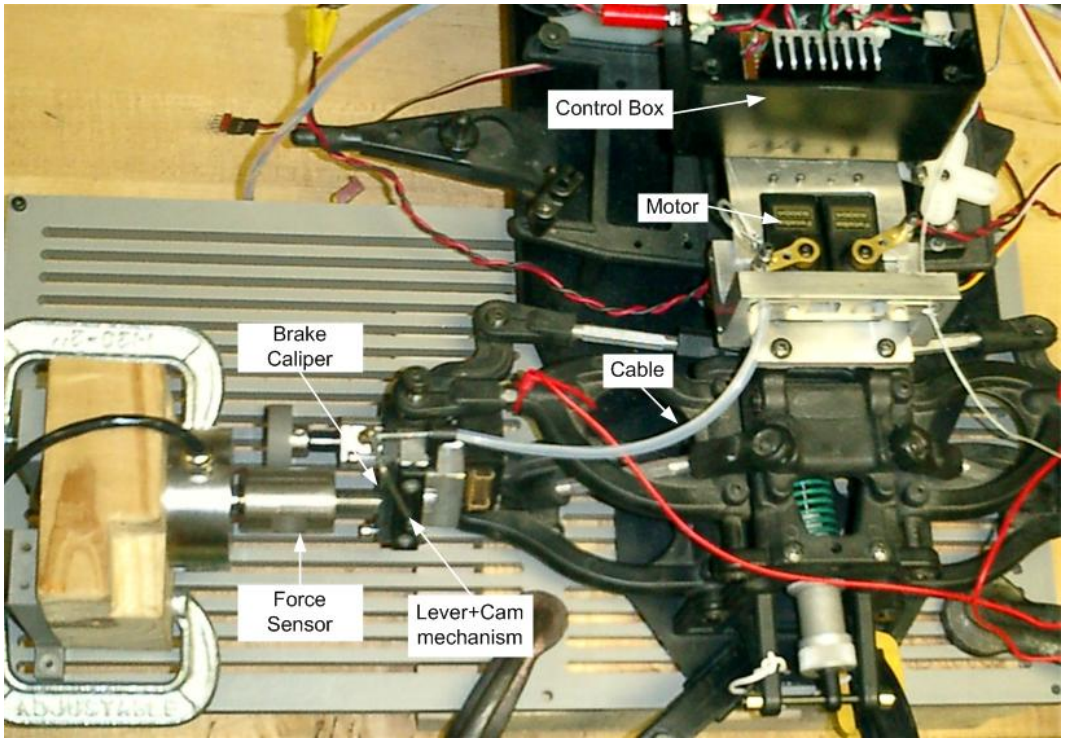


Figure 3.7: Swept-sine testing of the Brake System.

output, is shown in Fig. 3.9. The magnitude and phase shift of the output signal was determined by means of a LabVIEW program operating on the window of data. The magnitude was calculated as the difference between the maximum and the minimum values[1] in one cycle and averaging it over all the cycles in the data window (which was chosen by inspection to cover at least

[1]The 'amplitude' of a sine wave is defined as the difference between the maximum and the *average* values of the waveform. However, in this analysis, since it was easier to determine the extreme values from the test results, the magnitude is taken as the difference between the maximum and the mininum values (i.e., twice the amplitude). The magnitude portion of the Bode plots is thus obtained as the ratio of the output and the input waveform magnitudes, expressed in $dB$.

10 cycles). The phase shift (in degrees) was calculated from the time lag of the output over the input '$\Delta t$' using the relation, $\varphi = 360 \cdot f \cdot \Delta t$.

In order to determine the brake system parameters (system order, corner frequencies, gain) further experiments were carried out on the system components. The experiment to estimate the DC motor torque constant revealed that stiction in the motor gear drive created a deadzone in the motor operation characteristics. Frequency response testing of the motor showed that it is an underdamped second order system. From the Bode plot of the brake system, we see that the phase shift, $\varphi$, appears to approach -270$^o$ asymptotically. Since static nonlinear components affect only the magnitude and not the phase response of the system (all except 'hysteresis' [17], and it can be reasonably assumed that the brake system does not demonstrate hysteretic characteristics), the system can be considered to be of III-order. Furthermore, on account of its design, the cable-lever-cam mechanism intrinsically exhibits deadzone and saturation characteristics. The brake system can therefore be thought of as a juxtaposition of linear dynamical subsystems of order 'III' (i.e., the system can be described by $3^{rd}$ order ODEs) and static nonlinearities as shown in Fig. 3.10. The motor is represented in terms of its torque constant, $K_m$, natural frequency, $\omega_n$ and damping coefficient, $\zeta$ all of which have been estimated from the motor Bode plots. The transmission mechanism is quantified in terms of a gain, $K$, and time constant, $\tau$. The terms $\Delta_1$ and $\Delta_2$ correspond to the motor and mechanism dead zone parameters respectively, while $S$ is the mechanism saturation limit. Identifying these terms would then completely characterize the brake system.

The parameters of the nonlinearities are estimated from their describing function approximations. The describing function of a nonlinear element

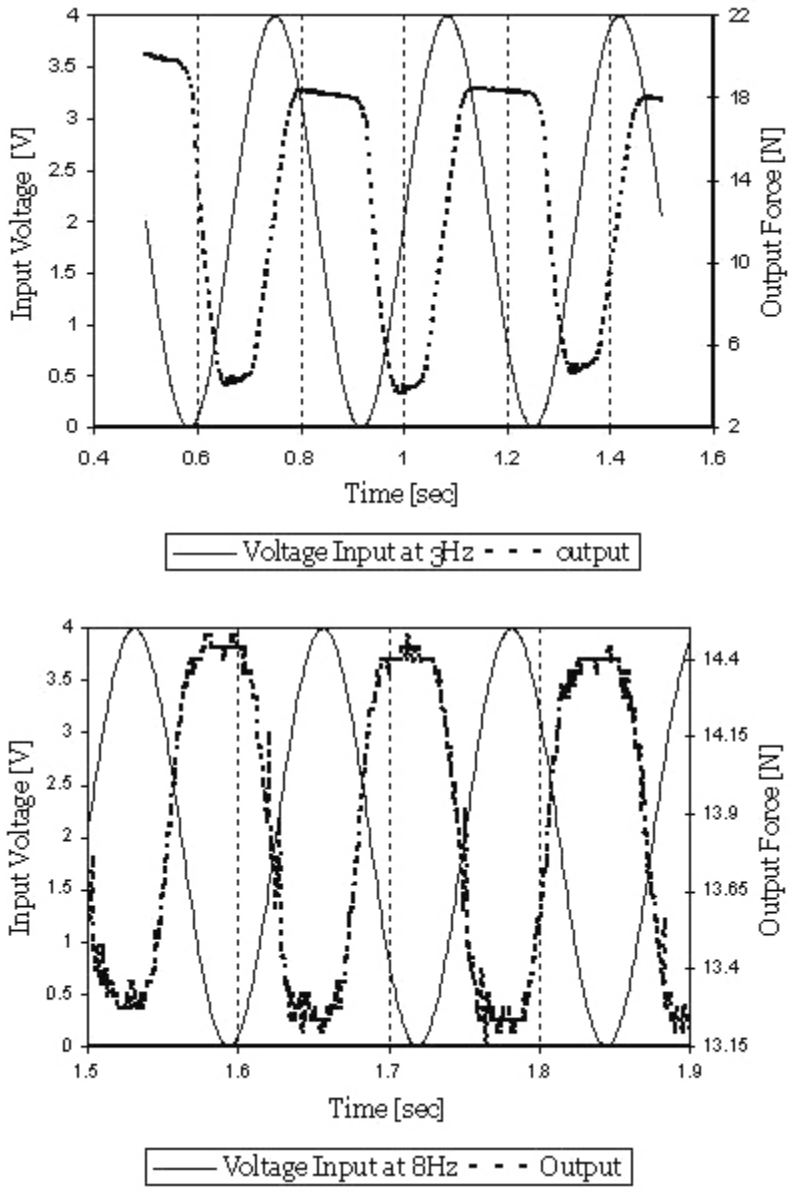


Figure 3.8: Sample Frequency Response Test Results.

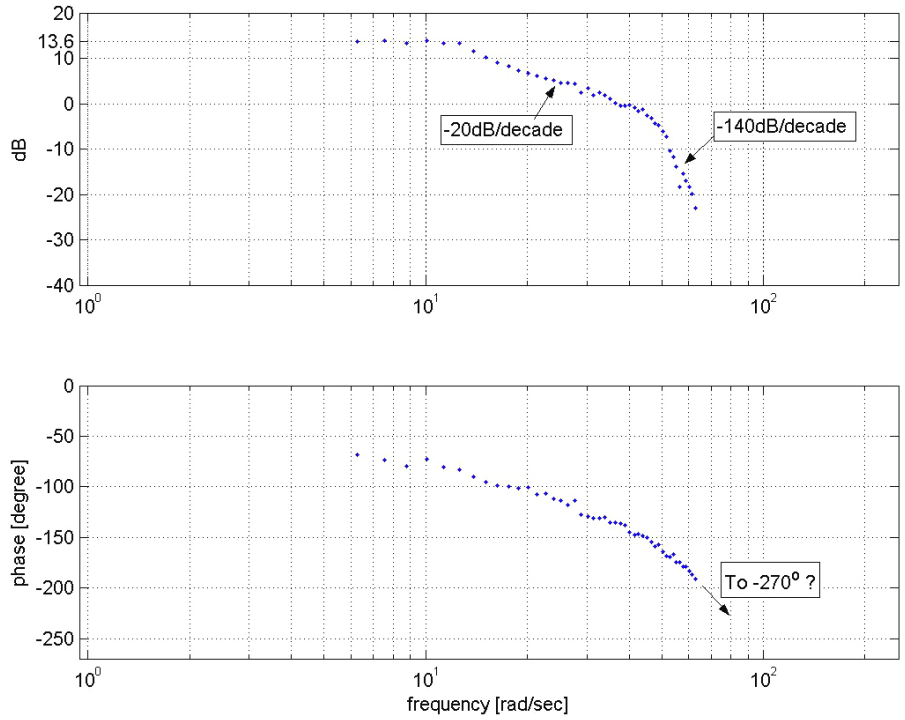


Figure 3.9: Bode Plot of the Brake System (before re-design).

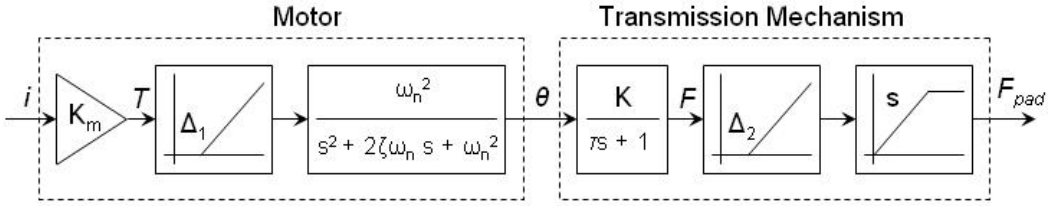


Figure 3.10: Brake System Model.

is defined to be the complex ratio of the fundamental harmonic component of the output to the input [17]. As the brake system has 'low-pass' characteristics, it can be assumed that the higher harmonics of the output are very much

attenuated and hence insignificant. Equation (3.3) gives the describing functions for dead zone($N_1$) and saturation($N_2$) effects. The output depends only upon the magnitude of the input and not on the frequency as the nonlinear elements do not store energy.

$$\begin{aligned} N &= \tfrac{Y}{X}\angle 0^o \\ N_1 &= m - \tfrac{2m}{\pi}\left[sin^{-1}\left(\tfrac{\Delta_1}{X}\right) + \tfrac{\Delta_1}{X}\sqrt{1-\left(\tfrac{\Delta_1}{X}\right)^2}\right] \\ N_2 &= \tfrac{2m}{\pi}\left[sin^{-1}\left(\tfrac{S}{X}\right) + \tfrac{S}{X}\sqrt{1-\left(\tfrac{S}{X}\right)^2}\right] \end{aligned} \tag{3.3}$$

These relations can be used in conjunction with the transfer functions of the linear dynamic elements to obtain a Bode plot for the linearized brake system. The parameter values can be adjusted by trial-and-error to match the analytic Bode plot with the one determined experimentally. The number of trials to adjust the parameters can be reduced by estimating the range of the parameters from the experimental data. For instance, the saturation limit, $S$, can be estimated from Fig. 3.6 to be in the range of $(14 \leq S \leq 20)N$. Fig. 3.11 shows the experimentally determined data points for the magnitude and phase difference plots superimposed with its analytical approximation, determined using the transfer function of the entire system. The numerical values of the parameters are listed in table 3.1.

The model obtained by the above experimental procedure provides insights about the bond graph model (derived in Sec. 3.2.1) of the system. Using the knowledge of the system order (the order of the denominator polynomial of the system transfer function), the dominant dynamics in the system can be identified in the bond graph and the components with fast dynamics (namely, the caliper pad stiffness, the motor inductance etc.,) can be neglected.

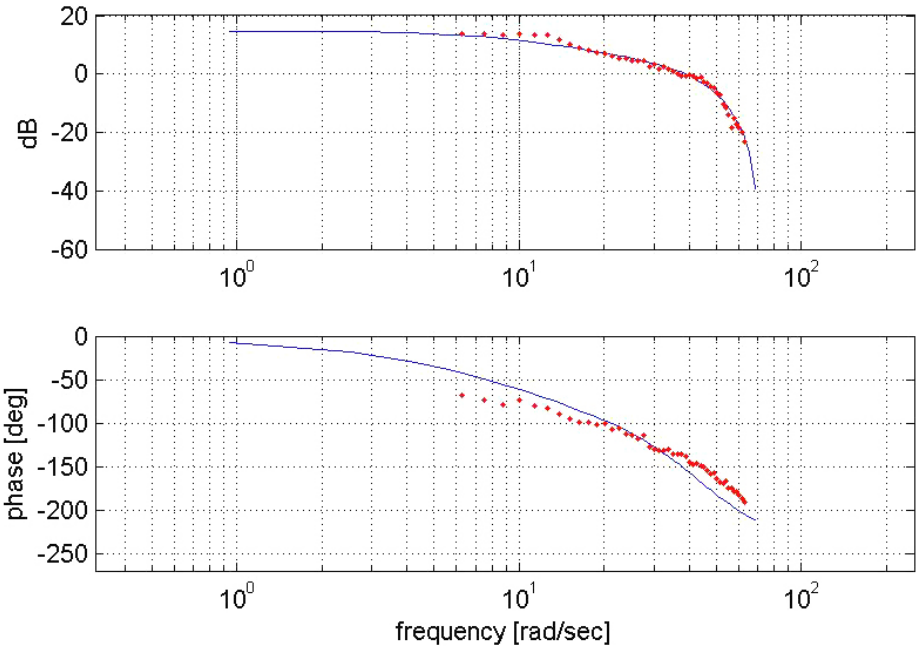


Figure 3.11: Bode Plot of the Brake System via Describing Function analysis.

Table 3.1: Frequency Response Data Model Parameters

| *Parameter* | *Value* | *Units* |
|---|---|---|
| $K_m$ | 0.88 | $Nm/A$ |
| $\omega_n$ | 7 | $Hz$ |
| $\zeta$ | 0.55 | |
| $\Delta_1$ | 0.1134 | $Nm$ |
| $K$ | 90 | |
| $\tau$ | 0.66 | $sec$ |
| $\Delta_2$ | 1 | $N$ |
| $S$ | 15 | $N$ |

## 3.3 Brake System Re-Design

This section discusses the efforts made to improve the performance of the brake system on the scale test vehicle. The objective and approach are developed first, followed by an outline of the specific steps undertaken to achieve the objective and finally, a discussion of the outcome of the efforts is presented.

### 3.3.1 Objective and Approach

It was established in Sec. 3.1 that the speed of response of the brake system is crucial for the ABS action, and that for the test vehicle the required bandwidth is $\approx 136Hz$. However, the frequency response model of the brake system revealed that its bandwidth is $\approx 15rad/sec$ (i.e., $2.5Hz$). It is then clear that in order to ensure effective ABS action, the dynamic response of the brake system on the test vehicle has to be substantially improved. With this objective, the probable concepts which can achieve it are discussed next.

One approach is to design a completely new brake system which would satisfy the bandwidth requirements. The brake system can be modeled after full-sized vehicle disk brake systems [20], by installing the brake actuator (i.e., the DC motor) in the vicinity of the brake calipers so that it acts directly on them. Then by choosing a DC motor of sufficiently high bandwidth, the brake system performance would be improved.

The second approach is to redesign the brake system. The redesign efforts could be at component-level, to modify the system components, e.g., replacing the cable, lever and cam mechanism by a different one. System-level redesign is also possible, using classical control techniques like employing PID control, lead/lag compensator, pole-placement method etc., to alter the system

behavior. This approach is adopted here. The brake system or the plant is assumed to be 'unalterable'. Any systemic modifications are limited to those that serve to make the system response more deterministic by eliminating and/or minimizing the static nonlinearities that were identified in the previous section. Once the system is physically linearized, simple lead-compensator is designed to improve the system bandwidth.

This system-level redesign procedure has the benefit that it requires only minor modifications to the system which can be quickly executed. The compensator transfer function can be conveniently implemented in software and the system performance can be greatly improved by simply adjusting the compensator parameters. The flipside is that, in order to realize the compensator, the system needs to operate in a closed-loop, which requires the use of a force sensor to measure the system output.

The steps of the brake system redesign are listed next. The improvement in performance is verified from the Bode plot of the system augmented with the compensator.

### 3.3.2 Tasks

The brake system was shown to possess a deadzone effect in the motor gear drive and, deadzone and saturation in the force transmission mechanism. The design changes that were implemented to offset these static nonlinearities are listed below. While it is difficult to determine the exact benefits of the changes made analytically, the improved system behavior is verified by frequency response studies similar to that carried out in Sec. 3.2.2.

1. The cable return spring was replaced by a stiffer one. This reduces the

effect of stiction in the motor gear drive, besides providing better brake release characteristics.

2. The freeplay in the mechanism was removed by providing a rigid joint between the cable and the lever. This minimizes the deadzone in the system operation region.

3. The cable shielding was replaced by a plastic casing to remove the Coloumb friction effect in the mechanism.

4. Additional return springs were included between the brake pads, thereby eliminating any deadzone effects.

Following the implementation of the above changes, the brake system was subjected to a swept-sine test again to determine its frequency response characteristics. As before, the amplitude of the input sinusoidal voltage signal was held constant and the frequency was swept from $0.1Hz$ to $10Hz$ in steps of $0.25Hz$. Fig. 3.12 shows the data points of the amplitude and phase difference of the brake system after re-design and the linear III-order system approximation to the data points. The approximation model fits the data points very well for the magnitude ($dB$) plot but not so for the phase difference. This is because the measurement of phase difference is error-prone [17] and the approximation of the system output by the fundamental component of the output holds very well only for the magnitude and not for the phase difference. It will be shown in Chapter 4 by simulation and testing, that this model approximation works well. It can then be inferred that the changes introduced into the system have been effective in mitigating the effects of the static nonlinearities. The parameters of the III-order approximation model are listed in table 3.2.

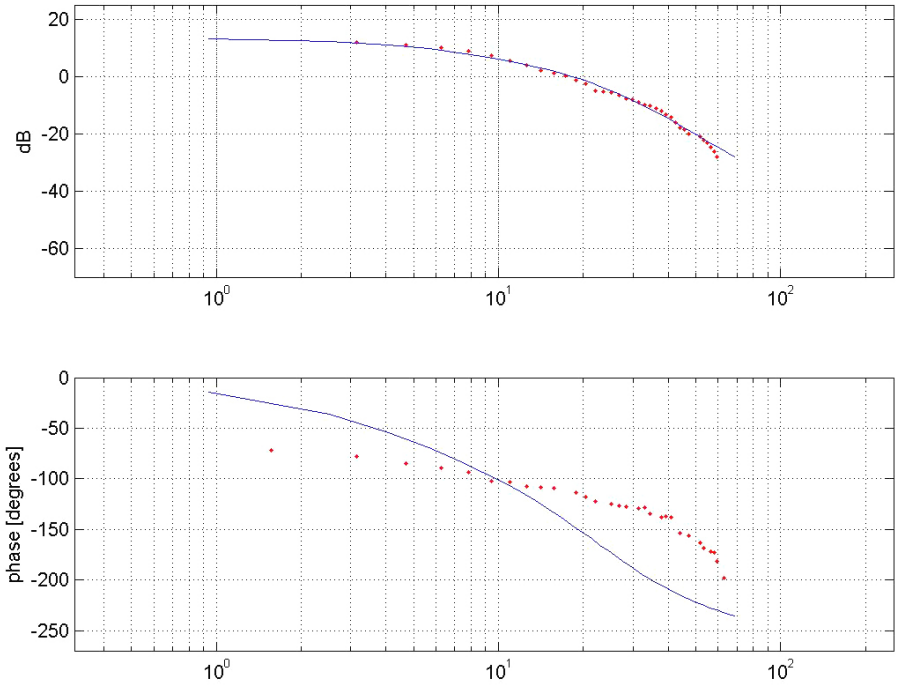


Figure 3.12: Bode Plot of the Brake System after re-design.

Table 3.2: Re-designed Brake System Parameters

| *Parameter* | *Value* | *Units* |
|---|---|---|
| $\omega_n$ | 3.75 | $Hz$ |
| $\zeta$ | 0.75 | |
| $K$ | 28.5 | |
| $\tau$ | 1.25 | $sec$ |

The transfer function of the linearized system is then given by,

$$\begin{aligned} G_p(s) &= \frac{K \cdot \omega_n^2}{(\tau \cdot s + 1)\left(s^2 + 2 \cdot \zeta \cdot \omega_n \cdot s + \omega_n^2\right)} \\ &= \frac{15822}{(0.2 \cdot s + 1)\left(s^2 + 35.34 \cdot s + 555.16\right)} \end{aligned}$$

### 3.3.3 Compensator Design

In order to further improve the system performance, a lead compensator will be realized to work in series with the system. The lead compensator will serve to improve the system bandwidth by adding a suitable phase lead angle [17]. The systems will work in a closed loop as shown in Fig. 3.13.

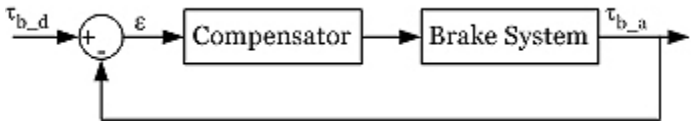


Figure 3.13: Closed-loop System with Compensator.

Following the 'root-locus' approach to compensator design, its transfer function is chosen so that the 'zero' cancels the open-loop 'pole' on the real axis of the system. The compensator 'pole' is placed far to the left of the pair of complex conjugate poles of the system, thereby making the dynamics of the conjugate pole pair dominant. The gain of the compensator is adjusted by trial-and-error via simulation. The resulting transfer function for the compensator is,

$$\begin{aligned} G_c(s) &= K_c \cdot \left( \frac{\tau_n \cdot s + 1}{\tau_d \cdot s + 1} \right) \\ &= 3 \cdot \left( \frac{0.125 \cdot s + 1}{0.01 \cdot s + 1} \right) \end{aligned}$$

It is seen that while one of the system poles was found at $s = -5$, the compensator zero which cancels it is not exactly located at the pole but is slightly to the left, at $s = -8$. This choice ensures that in the event the system pole is off from the predicted value, the compensator zero is still to the left of it, thereby ensuring stability of the system.

The combined open-loop transfer function of the system augmented with the compensator is given by $G_{ol}(s) = G_p(s) \cdot G_c(s)$. The closed-loop transfer function of the system is then,

$$G_{cl}(s) = \frac{G_{ol}(s)}{1 + G_{ol}(s)}$$

The Bode plot of the closed-loop system augmented with the compensator is shown in Fig. 3.14. The bandwidth of the open-loop system was found to be $15 rad/sec$, but that of the closed-loop system is seen to equal to $169 rad/sec$ ($\approx 27 Hz$). Any attempts to increase the system bandwidth further by increasing the compensator gain would lead to output saturation which is undesirable.

This completes the brake system re-design which accomplished the objective set forth. The effects of the static nonlinearities were minimized and the dynamic performance of the system was improved by augmenting it with a compensator. In the next chapter, the details of antilock brake system is discussed and two control schemes are designed for it and evaluated.

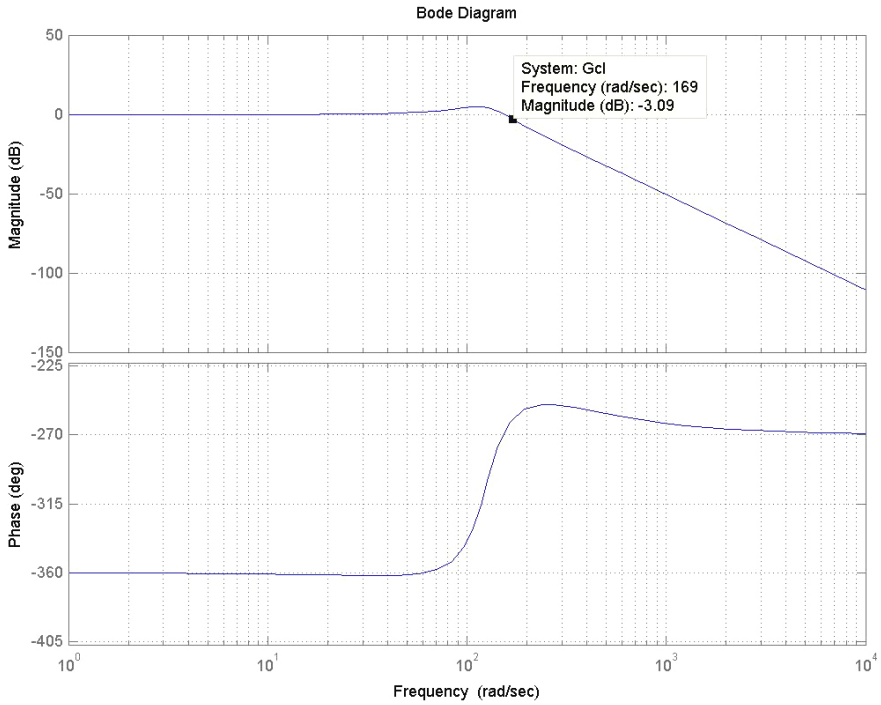


Figure 3.14: Bode Plot of the System augmented with the Compensator.

# Chapter 4

# ABS Control Prototyping

This chapter presents the results of prototyping two control schemes, namely, bang-bang control and sliding mode control, for antilock braking using the scaled vehicle test laboratory. The problem of antilock braking is described first, followed by a discussion of the design and simulation of the two control schemes. The performance of each control algorithm is evaluated using simulation results and hardware-in-the-loop testing (with the brake system as the hardware).

## 4.1 Tire-Pavement Interaction

The need for an antilock brake system arises due to the non-linear nature of the tire-pavement interaction. Hence an understanding of the interaction in both the longitudinal and the lateral directions is vital. When a braking torque is applied to a tire, due to its elasticity, the leading half of the tire tread stretches, before it enters the contact patch, as shown in Fig. 4.1. Thus the longitudinal tire travel will be greater when it is subjected to a braking torque than when it is free rolling. This difference leads to the 'longitudinal slip' which is defined as,

$$\lambda = \frac{V - \omega \cdot R_{tire}}{V} \tag{4.1}$$

where, $V$ is the longitudinal vehicle velocity, $\omega$ is the angular velocity of the tire and $R_{tire}$ is the tire radius.

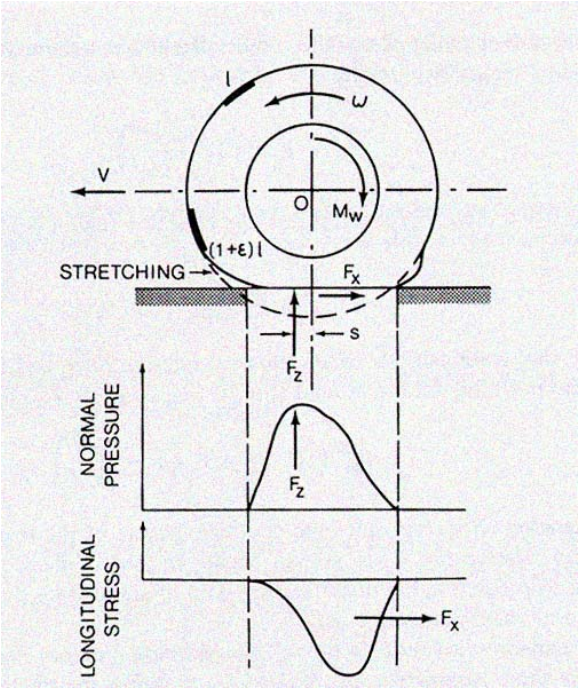


Figure 4.1: Behavior of tire under the action of brake torque [21].

Due to stretching of the tire i.e. 'slipping', a tractive force is developed by the tire which is proportional to the applied brake torque. This tractive force increases linearly with the applied torque within the elastic limit of the tire, corresponding to section $OA$ of the curve shown in Fig. 4.2. Once the tire starts to slide on the ground, the tractive force becomes a nonlinear function of the slip, entering section $AB$ of the curve. Any further increase in the torque then causes an unstable condition wherein the tractive force drops off from the peak value (which occurs at a slip value of approximately 0.2 for most surfaces) to a much lower value when the tire locks up (i.e., at slip of 1.0). The unstable region is shown by section $BC$ of the curve. The curve shows the variation of the coefficient of friction between the tire and the pavement,

which is defined as the ratio of the tractive effort to the normal load on the tire, with the tire slip. The friction coefficient is dependent upon a number of other factors like the tire tread, the road surface characteristics, presence of water on the surface, the vehicle speed and so on. Nevertheless, the nature of the curve is representative, with the other factors serving to scale the curve [4].

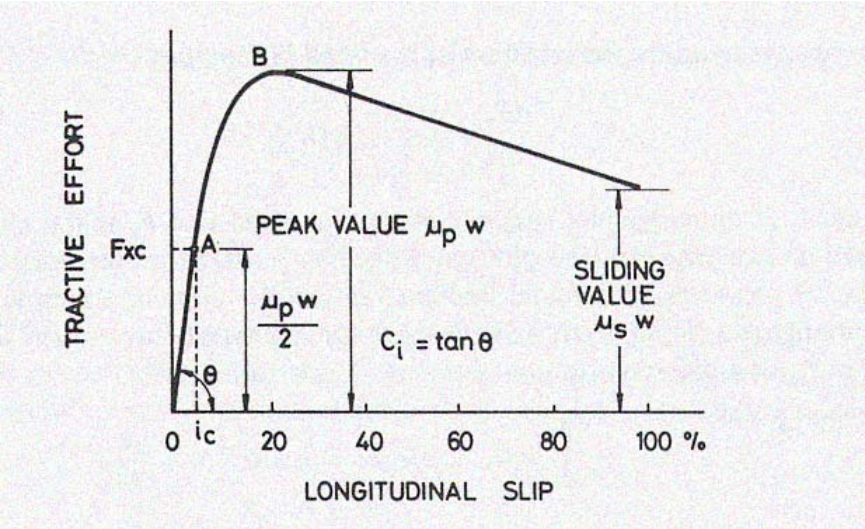


Figure 4.2: Variation of Tractive Effort with Longitudinal Slip [21].

In the absence of side forces, a rolling tire travels straight ahead along the tire plane. During a turning maneuver, however, the tire contact patch slips laterally while rolling such that its motion is no longer in the direction of the tire plane as shown in Fig. 4.3 [21]. The angle between the direction of motion of the tire and the tire plane is referred to as the 'sideslip' angle, $\alpha$. This lateral slip generates a lateral force at the tire-pavement interface. The force increases with the sideslip angle in an approximately linear fashion, up to about 4–6$^o$, beyond which it saturates to a value governed by the pavement and tire properties, as shown in Fig. 4.4. The slope of the curve at the origin

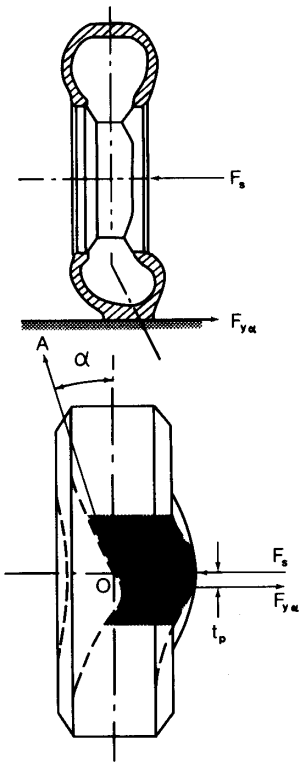


Figure 4.3: Tire Sideslip angle [21].

is termed as 'cornering stiffness' of the tire. The cornering stiffness of the tire is a measure of its capacity to respond to the steering wheel input during turning maneuvers. At any given instant, it is a function of the longitudinal slip of the tire and a typical relationship is shown in Fig. 4.5. When the tire is free rolling, the cornering stiffness of the tire is at its peak value which is determined by the tire properties (material, geometry etc.,). With increase in longitudinal slip during braking, the stiffness value drops and at tire lock-up state, it diminishes to a negligibly small value. This implies that the vehicle loses its directional control via steering when the front tires lock-up.

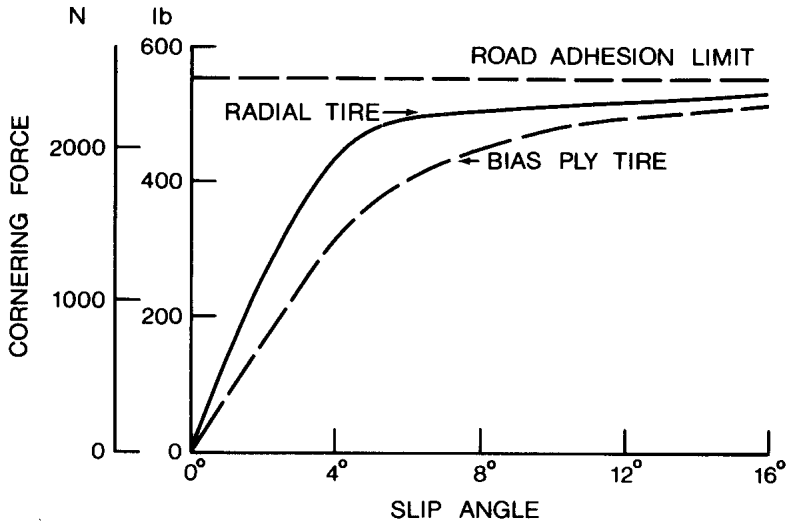


Figure 4.4: Variation of Lateral force with Sideslip angle [21].

It is clear from the above discussion that while tire lock-up may not have any drastic effect on the longitudinal stability of the vehicle, it gravely affects the lateral stability by causing the loss of directional response. The tire longitudinal slip must therefore be regulated at a value where the longitudinal friction coefficient is maximum (to minimize the stopping distance during braking) and the cornering stiffness has an appreciably large value (to retain steering response). The antilock brake system modulates the brake torque applied to the tire, based on the tire and the vehicle speed information and serves to regulate the tire slip in the region of desired operation.

Two control schemes will be developed in the next sections for the control of ABS and these will be evaluated by testing with the scaled vehicle. The plant, i.e., the vehicle, is modeled first and its state equations are obtained to facilitate the control design.

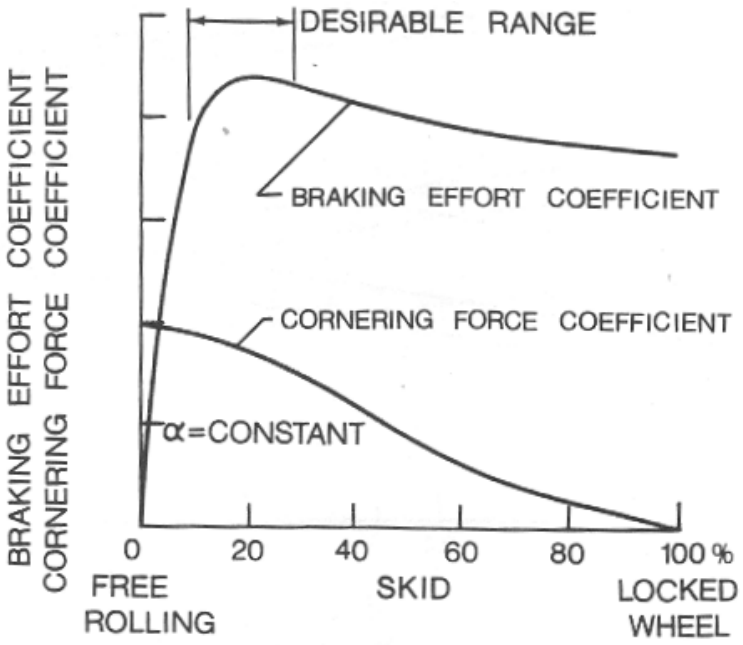


Figure 4.5: Variation of Cornering Stiffness with Longitudinal Tire Slip [21].

## 4.2 Vehicle Model

A mathematical model of the test vehicle (the plant) to facilitate the design of the control algorithms is developed in this section. A generic model to account for both the longitudinal and lateral vehicle dynamics will be considered so that the ABS action of the brake system can be evaluated in two maneuvers, straightline braking and braking while turning. A convenient approach is, to analyze the vehicle as a rigid body moving in an inertial frame and derive its dynamic equations of motion based on Euler's equations [24]. Simplifying assumptions are made to reduce the six degree-of-freedom Euler's equations into three degrees of freedom for the vehicle, which when augmented with the tire dynamics yield the state equations for the plant model.

The test vehicle is assumed to be a rigid body moving in a global inertial frame which has its origin at one corner of the test track, and the $X$-axis is aligned with the length of the track, $Y$-axis with the breadth of the track, and the $Z$-axis points into the ground. This is chosen so that the global axes are aligned with the body-fixed axis of the test vehicle when the vehicle is moving in a straight line along the length of the track. Fig. 4.6 shows the vehicle body-fixed axes according to the SAE vehicle axis system. To simplify the

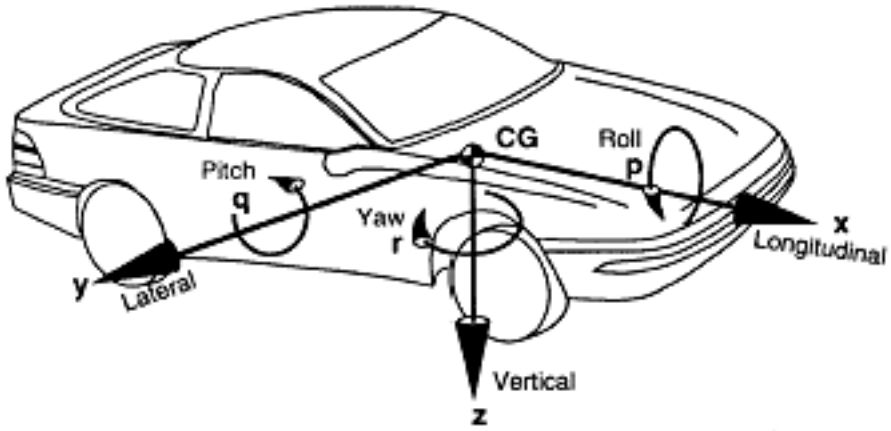


Figure 4.6: SAE Vehicle Axis System [23].

resulting state equations, a reasonable assumption that can be made is that the rotational motion of the test vehicle along the $X$-axis (vehicle roll) and the $Y$-axis (vehicle pitch) is insignificant on account of the stiff suspension system. Then, the 'bicycle model' can be used to account for simplified lateral and longitudinal vehicle dynamics thereby permitting the study of ABS action during panic braking conditions in both straight line and braking while turning maneuvers. A schematic of the bicycle model is shown in Fig. 4.7.

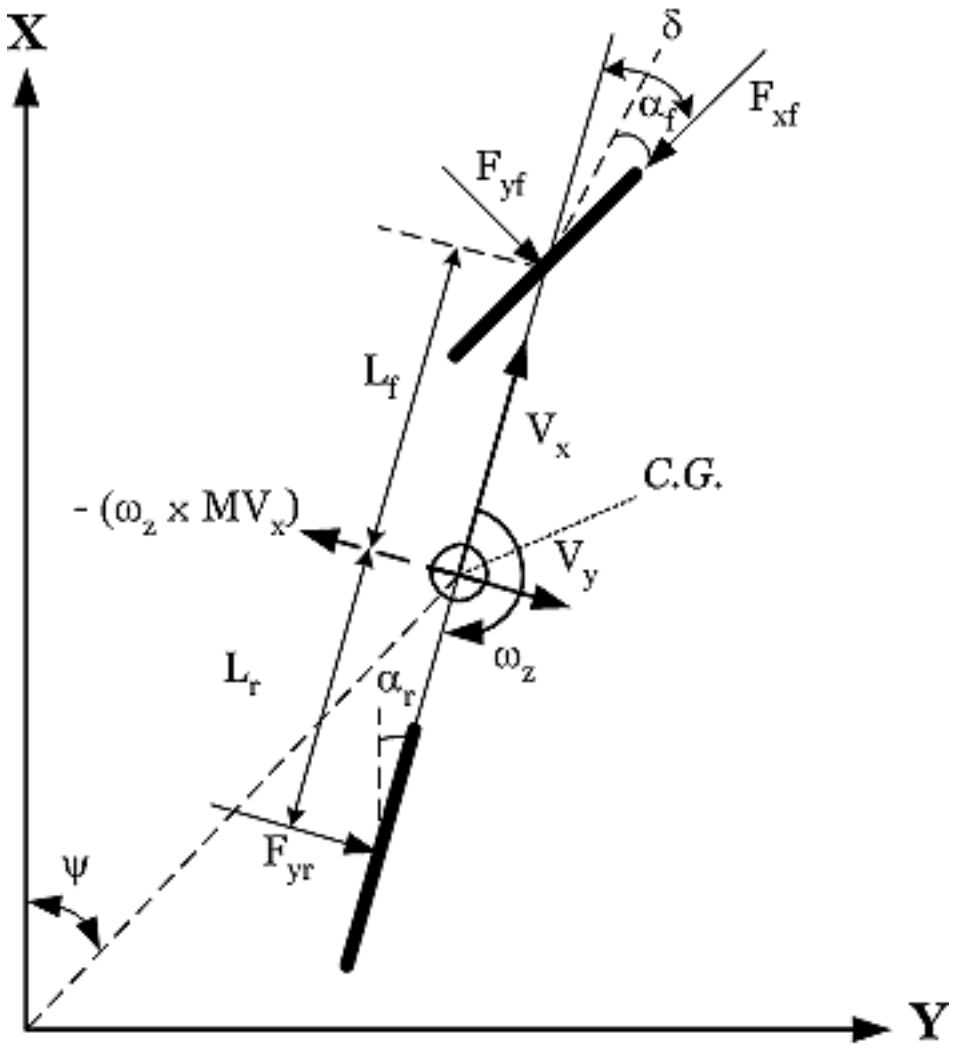


Figure 4.7: Linear Bicycle Model schematic.

Here, $\delta$ is the input steering angle (measured at the front tires), $\alpha_f$ and $\alpha_r$ are the front and the rear tire sideslip angles, respectively, and $L_f$ and $L_r$ are the distances of the vehicle $C.G.$ from the front and rear tires respectively.

The sideslip angles are determined from the kinematics of the system [21] and are given by,

$$\begin{aligned} \alpha_f &= \delta - \frac{L_f \cdot \omega_z + V_y}{V_x}, \\ \alpha_r &= \frac{L_r \cdot \omega_z - V_y}{V_x} \end{aligned}$$

The longitudinal force $F_{xf}$ on the front tires is determined as $F_{xf} = W_f \cdot \mu$, where $W_f$ is the weight of the vehicle on the front axle and $\mu$ is the friction coefficient of the tire-road surface interface and is a nonlinear function of the longitudinal tire slip, $\lambda$.

The component of the longitudinal velocity of the vehicle in the plane of the tire is $\frac{V_x}{cos(\delta)}$, and hence the longitudinal tire slip itself is calculated as,

$$\lambda = \left(1 - \frac{\omega_{tire} \cdot R_{tire} \cdot cos(\delta)}{V_x}\right) \tag{4.2}$$

The lateral forces at the front and rear tires, namely $F_{yf}$ and $F_{yr}$, are determined as $F_{y\dagger} = C_\dagger \cdot \alpha_\dagger$, where $\dagger$ stands for either $f$ or $r$ for 'front' and 'rear' respectively, and $C_f$ and $C_r$ are the cornering stiffness values for the front and the rear tires respectively.

The state equations for the model are obtained from the Euler's equations of motion of a rigid body by setting vehicle roll ($\omega_x$) and pitch ($\omega_y$) to zero [24]. The tire dynamics are described by Eqn. 3.1 (see Sec. 3.1). Combining the two sets of equations, a mathematical model of a vehicle undergoing

'braking while turning' can be defined as,

$$M \cdot \dot{V}_x = -F_{xf} \cdot cos(\delta) - F_{yf} \cdot sin(\delta), \tag{4.3}$$

$$M \cdot \dot{V}_y = F_{yf} \cdot cos(\delta) + F_{yr} - F_{xf} \cdot sin(\delta) - \omega_z \cdot M \cdot V_x, \tag{4.4}$$

$$J_z \cdot \dot{\omega}_z = F_{yf} \cdot cos(\delta) \cdot L_f - F_{xf} \cdot sin(\delta) \cdot L_f - F_{yr} \cdot L_r, \tag{4.5}$$

$$J_{tire} \cdot \dot{\omega}_{tire} = \left(\frac{1}{2}\right) \cdot F_{xf} \cdot R_{tire} - \tau_{brake}. \tag{4.6}$$

By setting the value of $\delta$ to be equal to zero or a constant value (positive or negative), the model can be used to study both straightline panic braking and braking while turning maneuvers.

It should be noted that the states $V_x$, $V_y$ and $\omega_z$ are defined for the body-fixed axes, and their global counterparts, $V_X$, $V_Y$ and $\omega_Z$, are given by applying the following transformation,

$$\begin{bmatrix} V_X \\ V_Y \\ \omega_Z \end{bmatrix} = \begin{bmatrix} cos(\psi) & -sin(\psi) & 0 \\ sin(\psi) & cos(\psi) & 0 \\ 0 & 0 & 1 \end{bmatrix} \cdot \begin{bmatrix} V_x \\ V_y \\ \omega_z \end{bmatrix}$$

Here, $\psi$ is the global yaw angle and is given by $\dot{\psi} = \omega_z$ when $\omega_x$ and $\omega_y$ are equal to zero [24]. The global velocity components upon integration yield the global position values $X$ and $Y$ of the vehicle during the maneuvers which are used to determine if the vehicle is negotiating the turn or is skidding off the track in simulations. During the actual laboratory tests, however, if there are no sensors to measure the lateral and the yaw velocities of the vehicle, only visual confirmation of the position attained by the vehicle is possible.

In the next section, the vehicle model is used to design two ABS control schemes.

## 4.3 ABS Control Design

A review of literature on the design of ABS control algorithms reveals that the vehicle model is augmented with the brake actuator model and the algorithms are designed by regarding the combined model as the plant [7],[8]. In this thesis, a cascade form of controller is realized. The ABS control schemes will be designed based on the vehicle model as the plant, independent of the brake system dynamics. The output of the ABS control schemes, the desired brake torque to be applied, will serve as the desired input to the brake system. The dynamic response of the brake system has been reshaped based on the ABS control scheme requirement using a lead compensator (see Sec. 3.3). A schematic of the cascade control is shown in Fig. 4.8.

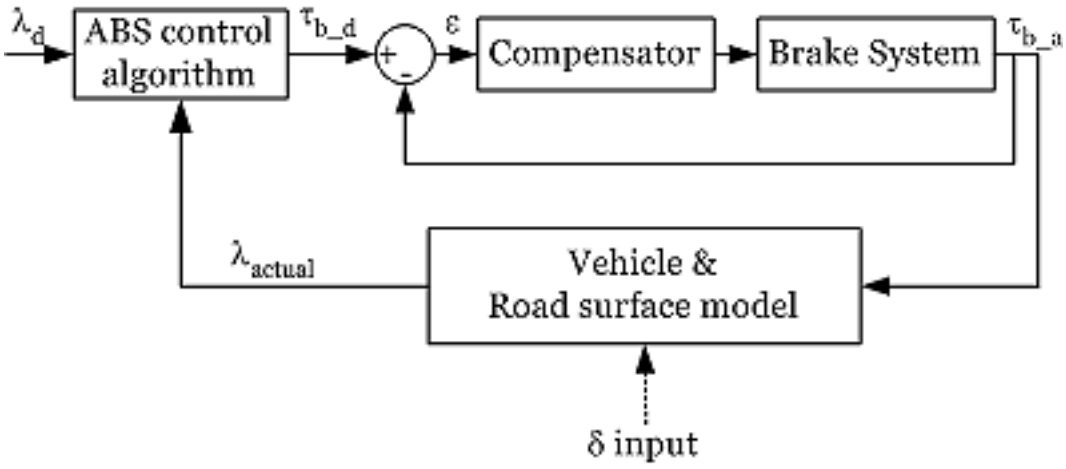


Figure 4.8: Schematic of the ABS Cascade Control Design.

The cascade control form is applicable to the ABS problem because the disk brake system dynamics are apparently independent of the vehicle and tire dynamics. The approach simplifies individual control design. The vehicle

model is tremendously simplified by not augmenting it with the brake system model. As the model order is reduced, control schemes that are based on the state space model of the plant (like optimal control, feedback linearization, sliding mode etc.,) are easier to realize and implement in real-time. Two control schemes for ABS, namely, 'bang-bang' type, and 'sliding mode' type, will be investigated here. They will be briefly introduced first, and then designed based on the vehicle model developed in Sec. 4.2. Their performance will then be evaluated by comparison with conventional braking. The comparison will be made based on their performance in the following scenarios,

1. Straightline panic braking maneuvers on a single surface
2. Straightline panic braking with a transition in the pavement surface from high PFC to low PFC[1]
3. Panic braking while turning.

The particular set chosen encompasses most situations commonly encountered in normal driving circumstances. As the antilock braking action brings about a reduction in the stopping distance, by regulating the tire slip at or near the value where the pavement traction is the best, the percentage improvement in the stopping distance ($SD$) determined as

$$\%\text{improvement} = \frac{SD_{ABS\,OFF} - SD_{ABS\,ON}}{SD_{ABS\,OFF}} \times 100$$

will be used to compare the two control schemes.

The simulation results from the panic braking scenario without any kind of ABS in straightline and in turning maneuver are shown in Fig. 4.9 and Fig. 4.10.

[1]PFC - Peak Friction Coefficient

**Straightline Panic Braking without ABS:-**

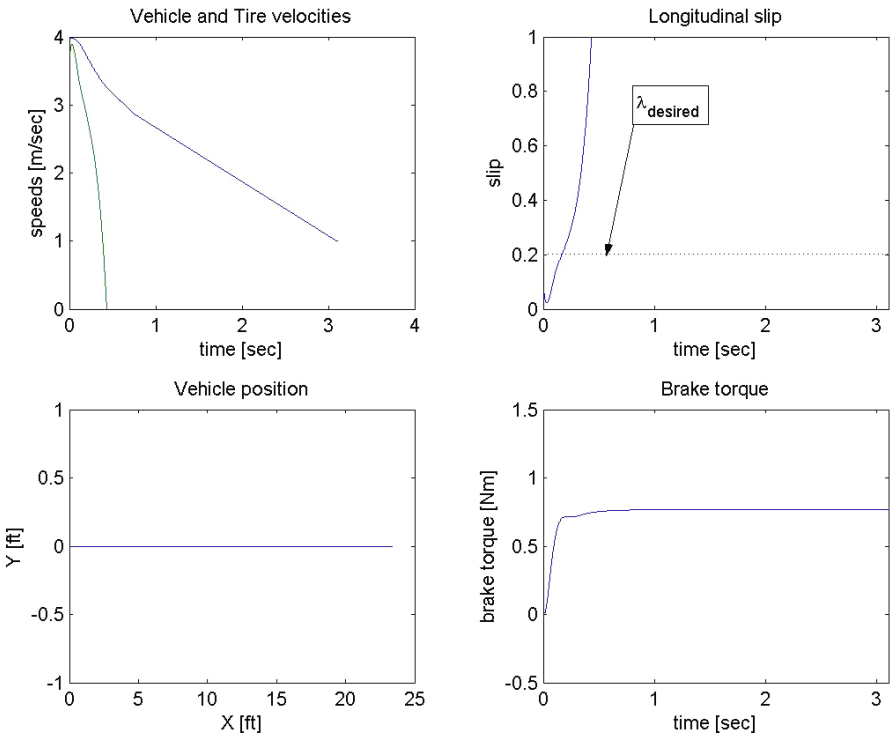


Figure 4.9: Simulation results for straightline braking without ABS, shows a step rise in the brake torque causing the tire to lock-up as indicated by the slip plot.

**Panic Braking while Turning without ABS:-**

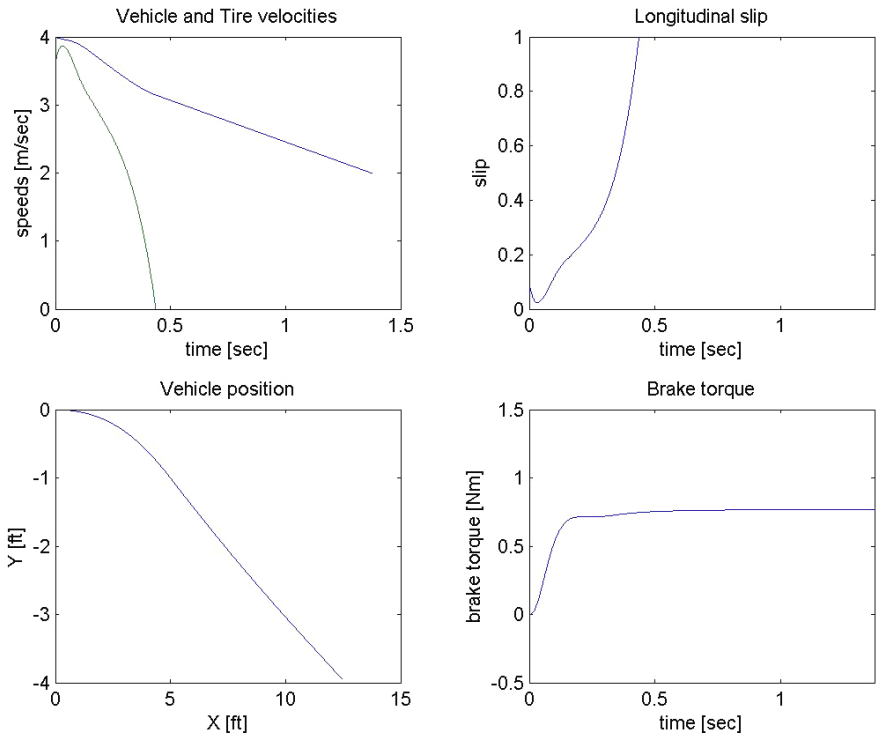


Figure 4.10: Simulation results for braking while turning without ABS, shows the vehicle skidding off the turn due to tire lock-up.

### 4.3.1 Bang-Bang Control

Bang-bang control is based on the principle that the system can be moved from one state to another in the shortest possible time by properly utilizing all the available control power at all times. In this sense bang-bang control is time-optimal (for a certain class of systems [17]). The control input to the system is 'switched' between the maximum and the minimum values based on some switching criterion. Because of the ease of implementation (achieved by using a simple 'relay') bang-bang type control is very popular. The switching is effected by a switching law depending upon the value of the states of the system. The locus on all the states at which switching occurs form a surface in the state-space called the switching curve/surface. For II-order systems the switching curve is determined conveniently using the 'phase-plane' design approach.

**Bang-Bang Control formulation for ABS**

For ABS, the longitudinal slip (which is defined in terms of the states of the system) can be chosen as the variable governing the switching law. As shown in Fig. 4.5, the desirable region for the longitudinal slip occurs in some range $\lambda \in \{\lambda_{low}, \lambda_{high}\}$. The control input, namely the brake torque $\tau_{brake}$, has to be switched between the maximum value, $\tau_{max}$, and the minimum value, 0, so as to keep the slip operating in the desirable region. Then, the switching law is defined as,

$$\tau^i_{brake} = \begin{cases} \tau_{max} & \lambda < \lambda_{low} \\ 0 & \lambda > \lambda_{high} \\ \tau^{i-1}_{brake} & \lambda \geq \lambda_{low} \;\&\; \lambda \leq \lambda_{high} \end{cases} \tag{4.7}$$

For convenience of analysis, by neglecting the steering angle input $\delta$, the order of the vehicle model becomes II, with the states $\{\frac{V}{R}, \omega\}$. Then the phase-plane

analysis of the system, with the switching law given in Eq. 4.7, is shown in Fig. 4.11, where $\frac{V}{R}$ is plotted along the $X$-axis and $\omega$ is plotted along $Y$-axis. Since the peak friction coefficient for most surfaces lies in the vicinity of 20 %

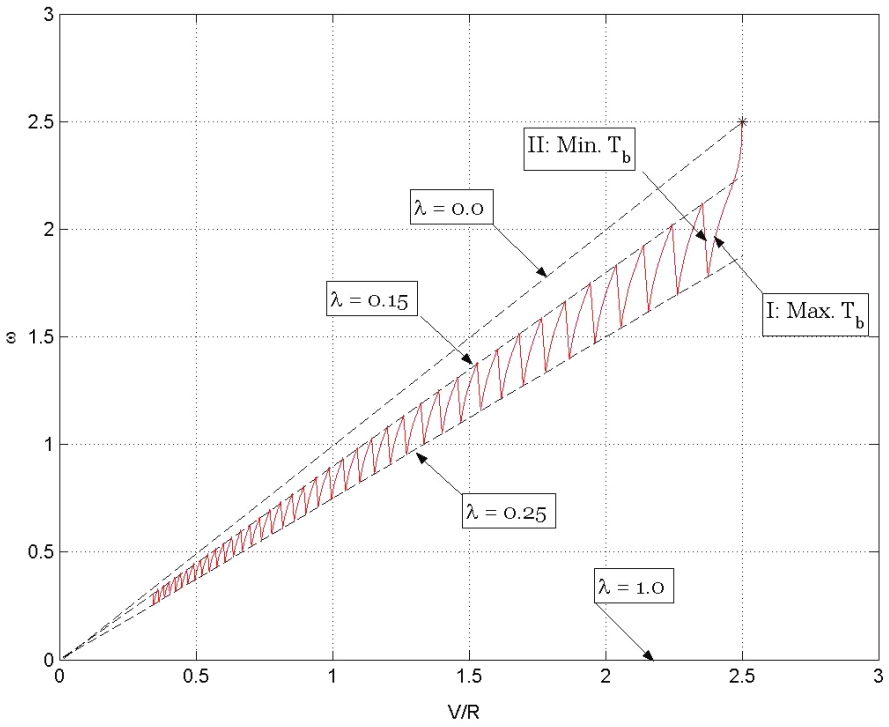


Figure 4.11: Phase portrait of the vehicle with Bang-Bang ABS.

longitudinal slip value, the region of operation of the slip value is chosen as $\lambda \in \{0.15, 0.25\}$. Then, by definition, the switching curves are $\lambda_{low} = 0.15$ and $\lambda_{high} = 0.25$. The system follows trajectory I when the maximum brake torque is applied and trajectory II when no brake torque is applied. By switching the control between the two, the slip is regulated in the desired region, thereby preventing the tires from locking up.

Once the ABS controller is designed, all the pieces of the cascade controller block diagram (see Fig. 4.3 are complete and ready for simulation. The vehicle model developed in Eq. 4.3 through 4.6, the ABS controller and the brake system loop are implemented in Simulink[2] for the purpose of simulation. The tire-pavement interface is set up as a 1-D look-up table ($\mu$ vs. $\lambda$). The bang-bang control scheme generates the control signal, i.e., the desired brake torque, for the closed loop brakes and compensator subsystem which then delivers the torque to the tires, causing the vehicle to brake. It was shown in Sec. 3.1 that, for the scaled test vehicle $\tau_{brake:max} > 1.145 \cdot \mu_{max}$, and hence, assuming $\mu_{max} \approx 0.75$ and accounting for the steady state error in the brake system, the maximum brake torque for the bang-bang control is chosen as, $\tau_{brake:max} = 2.5Nm$. The values of the slip parameters are selected as $i_{low} = 0.1$ and $i_{high} = 0.25$ as the slip range of $\{0.1, 0.25\}$ encompasses the desirable region of the $\mu$ vs. $\lambda$ variation for most pavement surfaces. For braking while turning simulation, the input steering angle $\delta$ is chosen to be equal to $+10^0$, which is the maximum angle by which the front tires can be steered in the scaled test vehicle. The positive angle results in the vehicle turning to the right as per the SAE vehicle axis definition. The simulation results for each of the three cases described in Sec. 4.3 are shown in Fig. 4.12, 4.13 and 4.14.

The simulation results indicate that by preventing tire lock-up, the ABS reduces the stopping distance and ensures that the vehicle retains steering response and negotiates the turn.

[2]The Mathworks Inc.,

**Straightline Panic Braking on a single surface with Bang-Bang ABS:-**

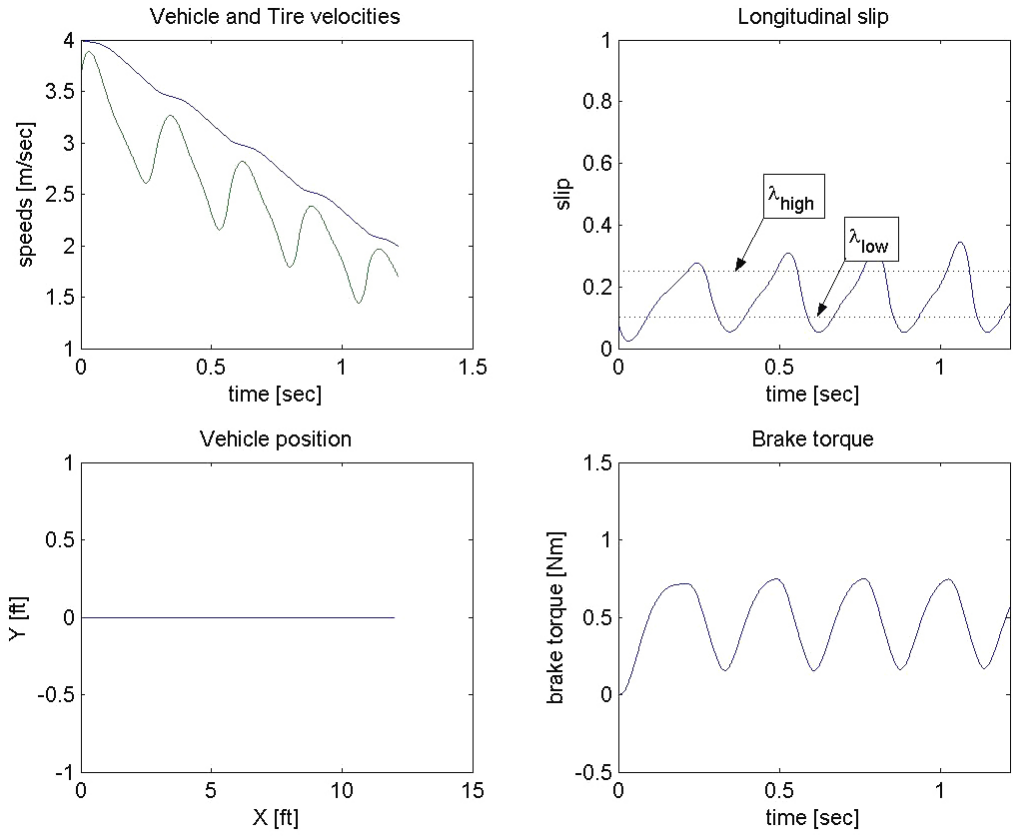


Figure 4.12: Simulation results for Straightline Braking with Bang-Bang ABS.

**Straightline Panic Braking with transition in the surface from a high $\mu$ to low $\mu$ value at time $T = 0.75$sec, with Bang-Bang ABS:-**

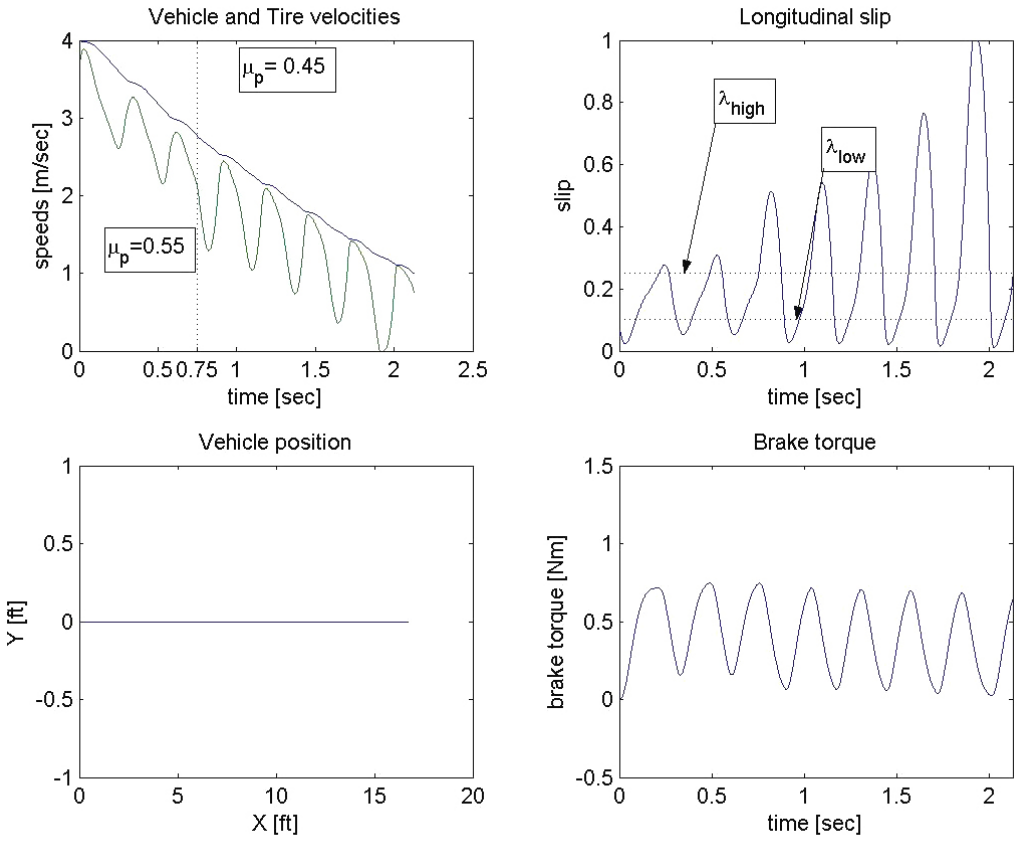


Figure 4.13: Simulation results for Braking with surface transition and Bang-Bang ABS.

**Panic Braking while Turning with Bang-Bang ABS:-**

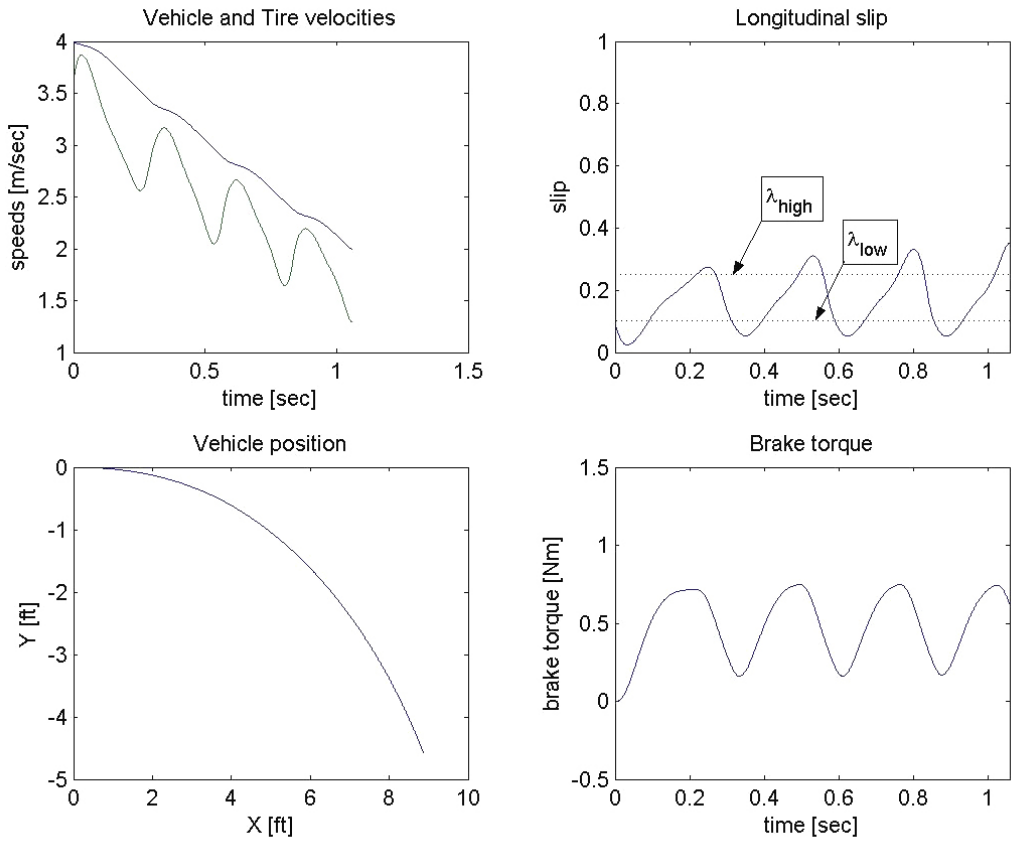


Figure 4.14: Simulation results for Braking while Turning with Bang-Bang ABS.

### 4.3.2 Sliding Mode Control

Sliding Mode control or Variable Structure control is a popular robust control scheme which finds widespread application in control of nonlinear systems. A simplified overview of the sliding control approach is mentioned in this section. The details can be found in Slotine [25].

The principle of sliding mode control is to convert the general $n^{th}$ order nonlinear system, of the form,

$$\begin{aligned} \dot{\mathbf{x}} &= f(\mathbf{x}) + g \cdot u, \\ y &= h(\mathbf{x}) \end{aligned}$$

into a 'first' order one, by defining a new output variable '$s$', in terms of the system output, $y$, and its desired value, $y_d$, as,

$$s = \left(\frac{d}{dt} + \Gamma\right)^{(r-1)} \cdot (y - y_d) \tag{4.8}$$

Here, $\Gamma$ is a sliding controller parameter and is representative of the actuator bandwidth [25], and $r$ is the relative order of the output (the control input '$u$' appears explicitly in its $r^{th}$ derivative). This definition ensures that $u$ appears in the $\dot{s}$ equation. The objective of the controller could be either to cause the output $y$ to 'track' $y_d$ (if $y_d$ is changing with time) or to 'regulate' $y$ at $y_d$ (if $y_d$ is a constant value). The objective is achieved by choosing a control law which causes $s \to 0$. The variable $s$ given by Eq. 4.8 simplifies to a function of the state variables $\mathbf{x}$ and the desired output $y_d$, i.e.,

$$s = p(\mathbf{x}, y_d)$$

and the equation $s = 0$ forms an $(n-1)^{th}$ order surface in state-space called the 'sliding surface'.

Then by differentiating $s$,

$$\begin{aligned} \dot{s} &= \frac{d}{dt}\{p(\mathbf{x}, y_d)\} \\ &\simeq q(\mathbf{x}, y_d, \dot{y_d}) + u \end{aligned}$$

By choosing the control law as,

$$u = \underbrace{-q(\mathbf{x}, y_d, \dot{y_d})}_{u_{eq}} \underbrace{-\eta \cdot sgn(s)}_{u_s}$$

the sliding surface dynamics become,

$$\dot{s} = -\eta \cdot sgn(s) \tag{4.9}$$

The discontinuous 'sgn' function, shown in Fig. 4.15, has a gain of $\infty$ at $s = 0$ so that $s$ is driven to zero (and hence the states are driven to the sliding surface) in a finite time, $t_{reach} = \frac{s(0)}{\eta}$ [26]. Once the sliding surface is reached, it is seen that $u_{eq} = 0$ or $u = u_s$, and if the states leave the surface (i.e., $s$ becomes non-zero), the switching control $u_s$ 'pushes' them back causing the states to stay on the sliding surface.

In the event of uncertainties in the system model, either parametric (system parameters) or structural (system order), the control input $u$ can be represented as

$$u = -\hat{q}(\mathbf{x}, y_d, \dot{y}_d) - \eta \cdot sgn(s),$$

where $\hat{q}$ is the approximate system model. Then,

$$\dot{s} = (q - \hat{q}) - \eta \cdot sgn(s)$$

By having $\eta > |(q - \hat{q})|$ it is seen that the control objective is achieved even in the presence of uncertainities. Thus sliding mode control assures robustness against uncertainties in the system model. Since estimating the extent

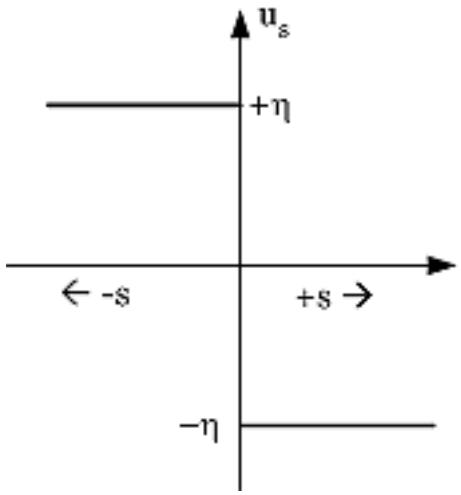


Figure 4.15: Discontinuous Control.

of $(q - \hat{q})$ can be tedious and sometimes error-prone, the value of the discontinuous control gain $\eta$ is made sufficiently large. But the flipside is that as $s \rightarrow 0$ because of the large gain it overshoots to the other side of the sliding surface causing the control to switch. This repeats and very high frequency switching of the control input occurs in the proximity of the sliding surface. This phenomenon is known as 'chattering' and can have either beneficial or deleterious effects on the system depending upon the application [25]. One of the ways to reduce chattering is to define a band around the sliding surface, wherein a smooth 'linear' approximation to the discontinuous control input $(u_s)$ is used, namely,

$$u_s = \begin{cases} -\eta \cdot sgn(s) & |s| > \Phi \\ -\eta \cdot \frac{s}{\Phi} & |s| \leq \Phi \end{cases}$$

This is shown in Fig. 4.16. Here, $2 \cdot \Phi$ represents the width of the band. While this robs the 'perfect' tracking/regulating ability of the sliding mode control (as $s$ can no longer be driven to zero identically), the high frequency chattering

is reduced. In the next section, the sliding mode control formulation will be

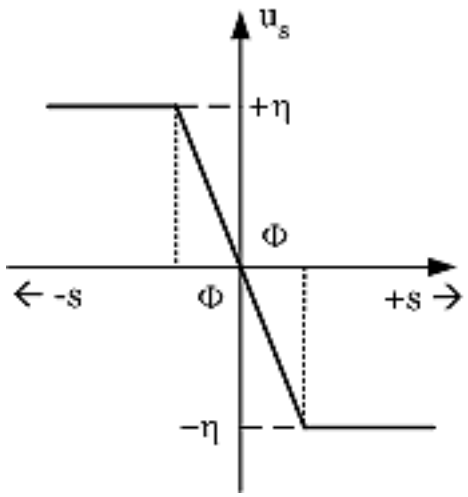


Figure 4.16: Smooth approximation to Discontinuous Control.

realized for the ABS control problem.

**Sliding Mode Control formulation for ABS**

In this section, a sliding mode controller will be realized to 'regulate' the tire slip value. For the purposes of ABS control, the longitudinal dynamics of the vehicle and the tire dynamics can be said to constitute the 'plant'. The lateral velocity and the yaw velocity can be regarded as outputs. The output of interest (which will be controlled), however, is the tire slip. For this reason, and for the sake of simplicity, the sliding mode controller will be designed to regulate the tire slip using the vehicle model developed in equations 4.3 through 4.6, by considering the input steering angle, $\delta$, to be zero. The controller will be extended later to include the case when $\delta$ is a non-zero constant. The plant

dynamics and the output equations are repeated here for $\delta = 0$.

$$\begin{aligned} M \cdot \dot{V}_x &= -W_f \cdot \mu \\ J_{tire} \cdot \dot{\omega}_{tire} &= \left(\frac{1}{2}\right) \cdot W_f \cdot \mu \cdot R_{tire} - \tau_{brake} \\ \lambda &= \left(1 - \frac{\omega_{tire} \cdot R_{tire}}{V_x}\right) \end{aligned} \tag{4.10}$$

To facilitate the derivation of the control law via sliding mode method analytically, a functional approximation will be made to the nonlinear relationhip between the tire-road friction coefficient and the tire slip value. The $\mu$ value is related to the tire slip $\lambda$ via the peak friction coefficient, $\mu_p$, offered by the surface and the tire slip value at which the peak friction occurs, $\lambda_p$ as shown in Eq. 4.11.

$$\mu(\lambda) = 2 \cdot \mu_p \cdot \lambda_p \cdot \left(\frac{\lambda}{\lambda_p^2 + \lambda^2}\right) \tag{4.11}$$

By choosing, $x_1 = V_x$, $x_2 = (\omega \cdot R_{tire})$ as the state variables and $y = \lambda$ as the output, the above equations can be re-written as,

$$\dot{x_1} = -g \cdot \left(\frac{L_r}{L}\right) \cdot \mu(\lambda) \tag{4.12}$$

$$\dot{x_2} = \left(\frac{1}{2}\right) \cdot g \cdot \left(\frac{M \cdot R_{tire}^2}{J_{tire}}\right) \cdot \left(\frac{L_r}{L}\right) \mu(\lambda) - \tau_{brake} \cdot \left(\frac{R_{tire}}{J_{tire}}\right) \tag{4.13}$$

$$y = \left(1 - \frac{x_2}{x_1}\right) \tag{4.14}$$

An important approximation in these equations is that the weight transfer onto the front axle on account of braking is neglected and the weight on the front axle is written simply as $W_f = W \cdot \frac{L_r}{L}$. This is a valid assumption in light of the fact that the height of the $C.G.$ is small compared to the wheelbase (see A.1 for the vehicle parameters listing). The increase in the weight on the front axle can

be expressed as $\Delta W_f = M \cdot a_x \cdot \left(\frac{H}{L}\right)$, where $a_x$ is the longitudinal deceleration, $H$ is the height of the $C.G.$ from the ground and $L$ is the wheelbase. The % increase will be $\frac{\Delta W_f}{W_f}$ which equals, $\left(\frac{a_x}{g} \cdot \frac{H}{L_r}\right)$. Since the ratio $\left(\frac{H}{L_r}\right) = 0.38$ for the scaled vehicle and the deceleration levels in $g$ units approximately equal the tire-road surface friction coefficient, which is another fraction between 0 and 1, the weight transfer effects can be neglected. Besides, as the test vehicle has front tire brakes, the weight transfer serves to improve the traction, thus aiding the controller in reducing the stopping distance.

By substituting, $K_L = \left(\frac{L_r}{L}\right)$, $K_J = \left(\frac{\left(\frac{1}{2}\right) \cdot M \cdot R_{tire}^2}{J_{tire}}\right)$, $K_R = \left(\frac{R_{tire}}{J_{tire}}\right)$ and $K_\mu = 2 \cdot \mu_p \cdot \lambda_p$, the state equations can be simplified as,

$$\dot{x_1} = -g \cdot K_L \cdot K_\mu \cdot \left(\frac{\lambda}{\lambda_p^2 + \lambda^2}\right) \tag{4.15}$$

$$\dot{x_2} = g \cdot K_J \cdot K_L \cdot K_\mu \cdot \left(\frac{\lambda}{\lambda_p^2 + \lambda^2}\right) - \tau_{brake} \cdot K_R \tag{4.16}$$

$$y = \left(1 - \frac{x_2}{x_1}\right) \tag{4.17}$$

Differentiating the output equation,

$$\begin{aligned} \dot{y} &= \frac{d}{dt}\left(1 - \frac{x_2}{x_1}\right) \\ &= \frac{\dot{x_1}(1-\lambda) - \dot{x_2}}{x_1} \end{aligned}$$

which upon simplification becomes,

$$\dot{y} = \frac{1}{x_1} \cdot \left[-gK_L K_\mu \cdot \left(\frac{\lambda \cdot (1-\lambda)}{\lambda_p^2 + \lambda^2}\right) - \left\{gK_J K_L K_\mu \cdot \left(\frac{\lambda}{\lambda_p^2 + \lambda^2}\right) - \tau_{brake} \cdot K_R\right\}\right]$$

As the control input, namely $\tau_{brake}$, appears in the *first* derivative of $y$, the relative order of the output, $r$, is **1** by definition [25]. Then, by defining the

sliding variable $s$ as,

$$\begin{aligned} s &= \left(\frac{d}{dt} + \Gamma\right)^{(r-1)} \cdot (y - y_d) \\ &= y - y_d \end{aligned}$$

it is clear that the sliding variable is a function of both the state variables. Here, $y_d$ is the desired slip value at which the tire slip must be regulated, and since it is a constant value, $\dot{y}_d = 0$.

Then, following the procedure outlined in Sec. 4.3.2,

$$\begin{aligned} \dot{s} &= \dot{y} \\ &= \frac{1}{x_1} \cdot \left[ -gK_L K_\mu \cdot \left( \frac{\lambda}{\lambda_p^2 + \lambda^2} \right) \{(1 - \lambda) + K_J\} + \tau_{brake} \cdot K_R \right] \end{aligned}$$

In order to have $\dot{s} = -\eta \cdot sgn(s)$, the control input $\tau_{brake}$ becomes,

$$\tau_{brake} = \left(\frac{\hat{x}_1}{\hat{K}_R}\right) \cdot \left[ \frac{g\hat{K}_L\hat{K}_\mu}{\hat{x}_1} \cdot \left( \frac{\hat{\lambda}}{\lambda_p^2 + \hat{\lambda}^2} \right) \left\{ (1 - \hat{\lambda}) + \hat{K}_J \right\} - \eta \cdot sgn(s) \right] \quad (4.18)$$

where the terms with the '$\hat{}$' represent the best *estimates* of the parameters on account of the uncertainty in the model.

In order to estimate the value of $\eta$, a positive-definite 'Lyapunov' function, $V$, is written in terms of 's' (and hence in terms of all the state variables), and a value is chosen which ensures that $\dot{V}$ is negative-definite (thereby making the system 'stable' according to Lyapunov's stability criteria [25]). Choosing $V = \frac{1}{2}\, s^2$ as the Lyapunov function, it then follows that,

$$\begin{aligned} \dot{V} &= s \cdot \dot{s} \\ &= \frac{(\lambda - \lambda_d)}{x_1} \cdot \left[ -gK_L K_\mu \cdot \left( \frac{\lambda}{\lambda_p^2 + \lambda^2} \right) \{(1 - \lambda) + K_J\} + \tau_{brake} \cdot K_R \right] \end{aligned}$$

Substituting for $\tau_{brake}$ from Eq. 4.18,

$$\begin{aligned}\dot{V} &= s \cdot \Bigg[ - \frac{gK_L K_\mu}{x_1} \cdot \left( \frac{\lambda}{\lambda_p^2 + \lambda^2} \right) \{(1-\lambda) + K_J\} \\ &\quad + \left( \frac{K_R}{\hat{K_R}} \right) \cdot \frac{g\hat{K}_L \hat{K}_\mu}{x_1} \cdot \left( \frac{\hat{\lambda}}{\lambda_p^2 + \hat{\lambda}^2} \right) \left\{ (1-\hat{\lambda}) + \hat{K}_J \right\} \\ &\quad - \left( \frac{K_R}{\hat{K_R}} \right) \cdot \left( \frac{\hat{x}_1}{x_1} \right) \cdot \eta \cdot sgn(s) \Bigg] \end{aligned} \tag{4.19}$$

It is clear from Eq. 4.19 that for $\dot{V}$ to be negative-definite, the discontinuous control gain $\eta$ has to be,

$$\begin{aligned}\eta &> \left( \frac{x_1}{\hat{x}_1} \right) \cdot \Bigg| \frac{g\hat{K}_L \hat{K}_\mu}{x_1} \cdot \left( \frac{\hat{\lambda}}{\lambda_p^2 + \hat{\lambda}^2} \right) \left\{ (1-\hat{\lambda}) + \hat{K}_J \right\} \\ &\quad - \left( \frac{\hat{K_R}}{K_R} \right) \cdot \frac{gK_L K_\mu}{x_1} \cdot \left( \frac{\lambda}{\lambda_p^2 + \lambda^2} \right) \{(1-\lambda) + K_J\} \Bigg| \end{aligned}$$

The actual value of $\eta$ is conveniently determined via simulation. To reduce chattering and to prevent the sliding mode controller from working in a 'bang-bang' fashion, a smooth approximation is made to the discontinuous control within a band of width $2 \cdot \Phi$ as outlined in Sec. 4.3.2.

The control input, $\tau_{brake}$, with sliding mode controller is, $\tau_{brake} = u_{eq} + u_s$, where,

$$\begin{aligned} u_{eq} &= \frac{g\hat{K}_L \hat{K}_\mu}{\hat{K}_R} \cdot \left( \frac{\hat{\lambda}}{\lambda_p^2 + \hat{\lambda}^2} \right) \left\{ (1-\hat{\lambda}) + \hat{K}_J \right\} \\ u_s &= \begin{cases} -\eta' \cdot sgn(s) & |s| > \Phi \\ -\eta' \cdot \frac{s}{\Phi} & |s| \leq \Phi \end{cases} \end{aligned} \tag{4.20}$$

Here, $\eta' = \left( \frac{\hat{x}_1}{\hat{K}_R} \right) \cdot \eta$.

In the event of braking while turning, when the input steering angle $\delta$ is not zero, the sliding mode controller designed in Eq. 4.20 will still work when

the value of $\delta$ is constant, and the longitudinal slip $\lambda$ is defined according to Eq. 4.2. The effect of steering on the vehicle model (given by Eq. 4.3 through Eq. 4.6) can be regarded as introducing parametric uncertainties (in the form of trigonometric functions of $\delta$) which are handled by the robust controller.

The sliding mode control for ABS is simulated with the parameters $\lambda_{desired} = 0.2$, $\eta = 25$ and $\Phi = 0.05$. The simulation results for the three cases are shown in Fig. 4.17, 4.18 and 4.19.

**Straightline Panic Braking on a single surface with Sliding Mode ABS:-**

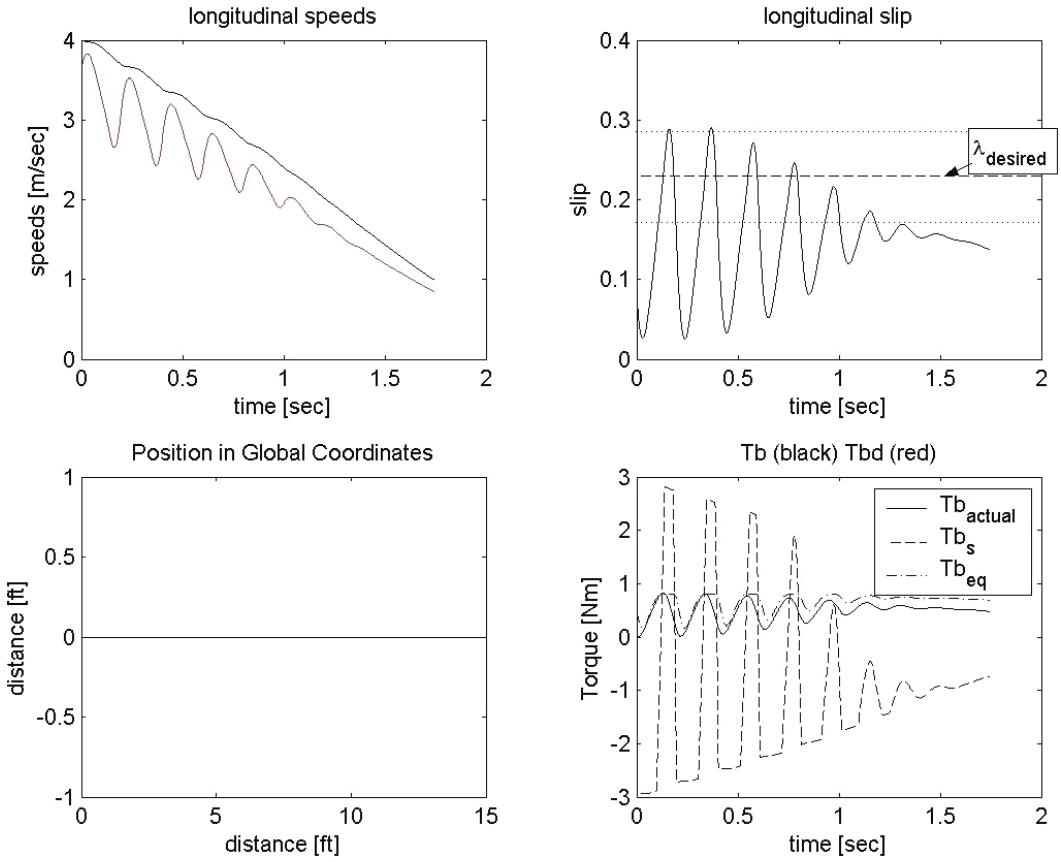


Figure 4.17: Simulation results for Straightline Braking with Sliding Mode ABS.

**Straightline Panic Braking with transition in the surface from a high $\mu$ to low $\mu$ value at time $T = 1.0$sec, with Sliding Mode ABS:-**

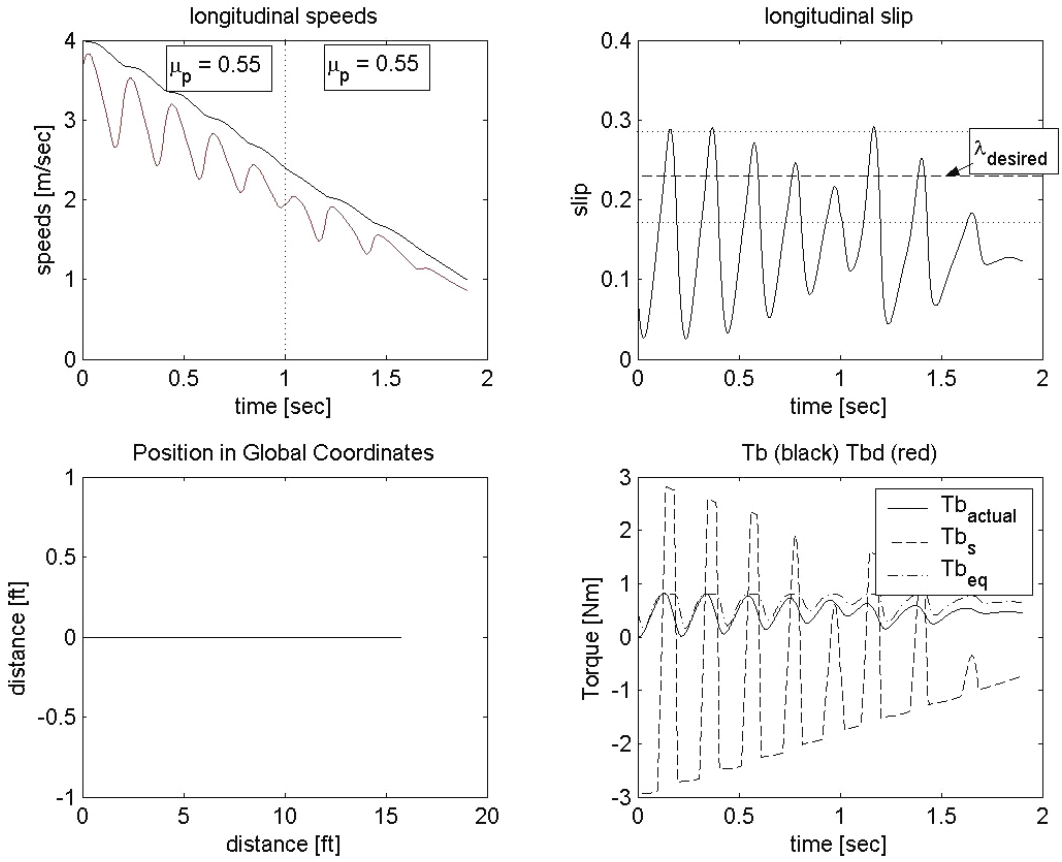


Figure 4.18: Simulation results for Braking with surface transition and Sliding Mode ABS.

**Panic Braking while Turning with Sliding Mode ABS:-**

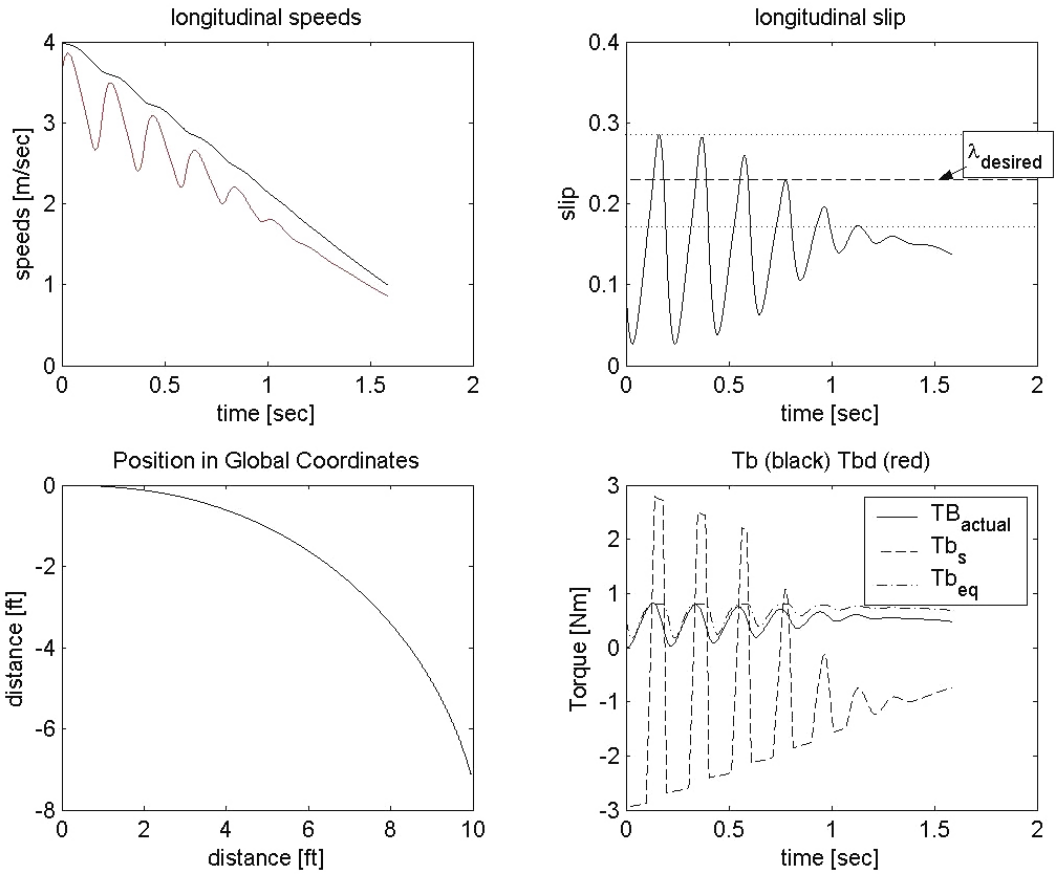


Figure 4.19: Simulation results for Braking while Turning with Sliding Mode ABS.

## 4.4 ABS Control Testing

This section describes the hardware-in-the-loop testing (HIL) of the control algorithms designed in the previous section.

According to the control prototyping process described in Sec. 2.2, the vehicle model, the tire-pavement interface characteristics, the brake system model (represented as a transfer function) and the ABS control algorithms were implemented in software (in MATLAB/Simulink) and the controller was fine-tuned via simulation. The entire Simulink model was then converted into a LabVIEW VI, thereby transferring the models from a simulation environment to a testing environment, using the Matlab Real-time Workshop and the LabVIEW Simulation Interface Toolkit. In order to perform HIL testing with the brake system, the brake system portion of the VI was replaced by DAQ VIs to interface with the data acquisition unit. The vehicle and the tire model, the pavement characteristics and the ABS controller are contained in the VI which runs on the real-time controller module. A setup identical to the one used for the swept-sine testing (see Fig. 3.7) was built for HIL testing. The desired brake torque specified by the ABS controller is output as a proportional voltage by the 'output DAQ VI' to the motor of the brake system. The force at the brake calipers is measured by a force sensor which is then read by an 'input DAQ VI' and converted to the equivalent brake torque. As the model is being run on real-time hardware, and data is being sampled every 1ms, which is nearly seven times the highest frequency found in the model (the bandwidth of the vehicle braking model for the scaled vehicle was found to be 136Hz, see Sec. 3.1) HIL testing is possible.

Five trials of testing were carried out for each of the three cases, with both bang-bang and sliding mode ABS. The test results with ABS for bang-

bang control for the three cases are shown in Fig. 4.20, 4.21 and 4.22. The results of sliding mode control ABS are shown in Fig. 4.23, 4.24 and 4.25.

The stopping distance was determined in each of the test cases between the start of braking ($V_x = 4.0\ m/sec$) and the instant when the vehicle velocity reached 2.0 $m/sec$, and was averaged over the five iterations. The stopping distance for conventional braking without ABS was also similarly determined. Table 4.1 lists the values and the percentage improvement over braking without ABS, for each of the cases. The next section discusses the results of HIL testing.

Table 4.1: Stopping distance (% improvement) with and without ABS: Simulation(S) and HIL Test(T) results

| *Scenario* | *Bang-bang ABS* | *Sliding Mode ABS* | *No ABS* |
|---|---|---|---|
| Straightline braking | | | |
| S | $3.66m$ (15%) | $3.32m$ (23%) | $4.30m$ |
| T | $3.38m$ (30%) | $2.79m$ (42%) | $4.82m$ |
| Surface transition | | | |
| S | $3.88m$ (26%) | $3.49m$ (33%) | $5.23m$ |
| T | $3.44m$ (35%) | $3.13m$ (41%) | $5.28m$ |
| Braking while turning | | | |
| S | $2.70m$ (29%) | $2.57m$ (32%) | $3.80m$ |
| T | $2.84m$ (53%) | $2.55m$ (57%) | $6.00m$ |

**HIL test results for Straightline Panic Braking on a single surface with Bang-Bang ABS:-**

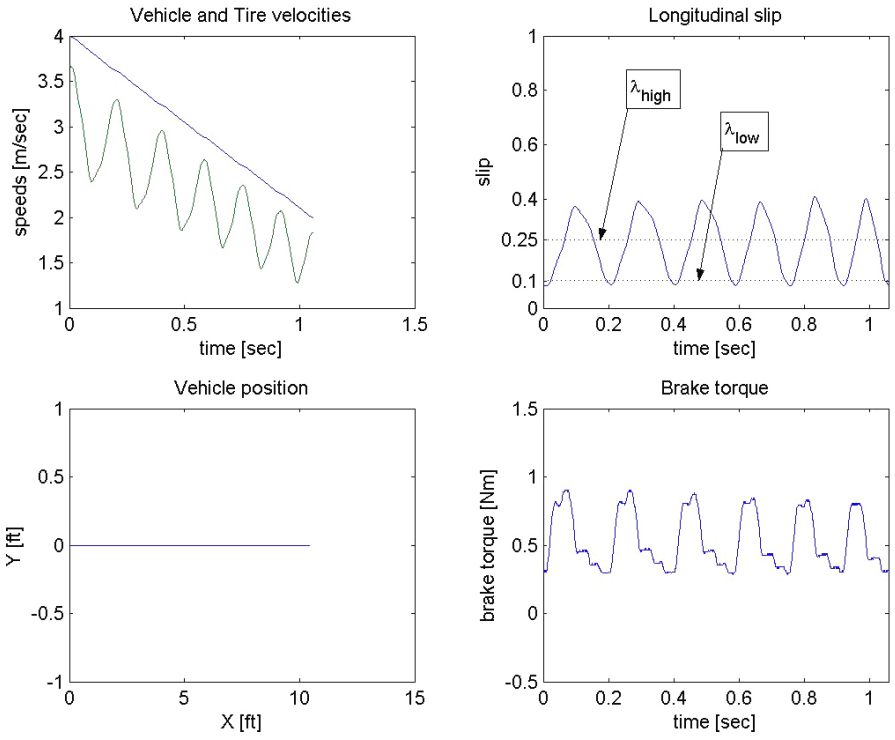


Figure 4.20: HIL test results for Straightline Braking with Bang-Bang ABS.

**HIL results for Straightline Panic Braking with transition in the surface from a high $\mu$ to low $\mu$ value at time $T = 0.75sec$, with Bang-Bang ABS:-**

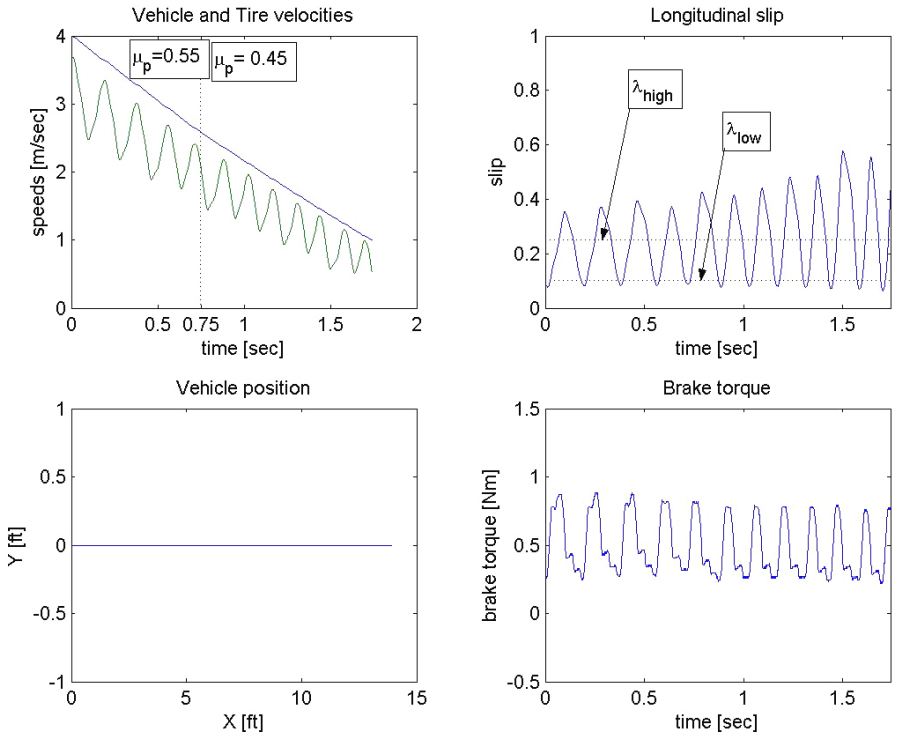


Figure 4.21: HIL test results for Braking with surface transition and Bang-Bang ABS.

**HIL test results for Panic Braking while Turning with Bang-Bang ABS:-**

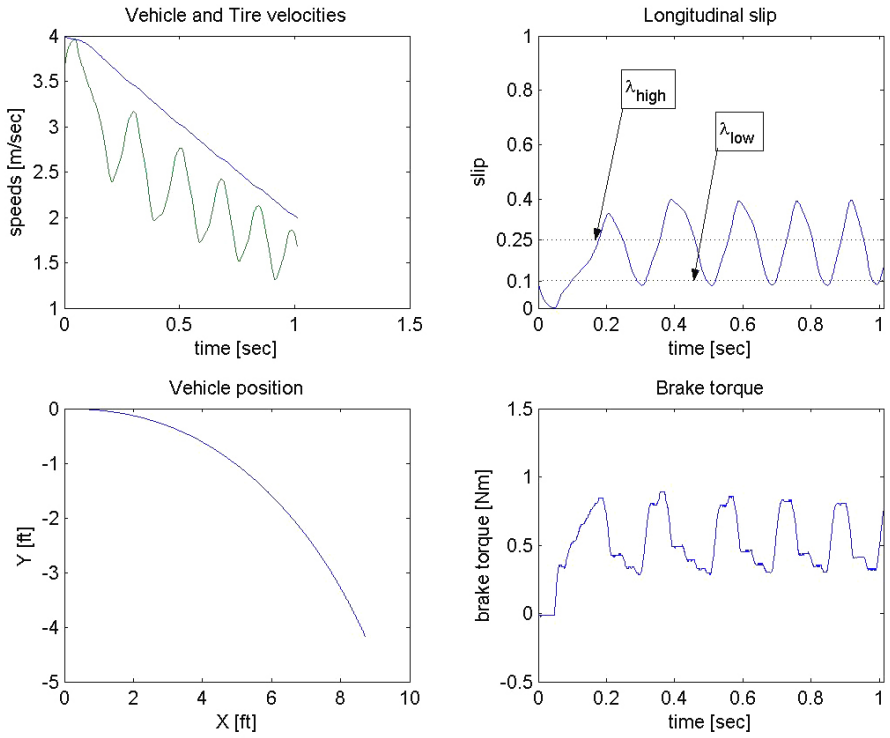


Figure 4.22: HIL test results for Braking while Turning with Bang-Bang ABS.

**HIL test results for Straightline Panic Braking on a single surface with Sliding Mode ABS:-**

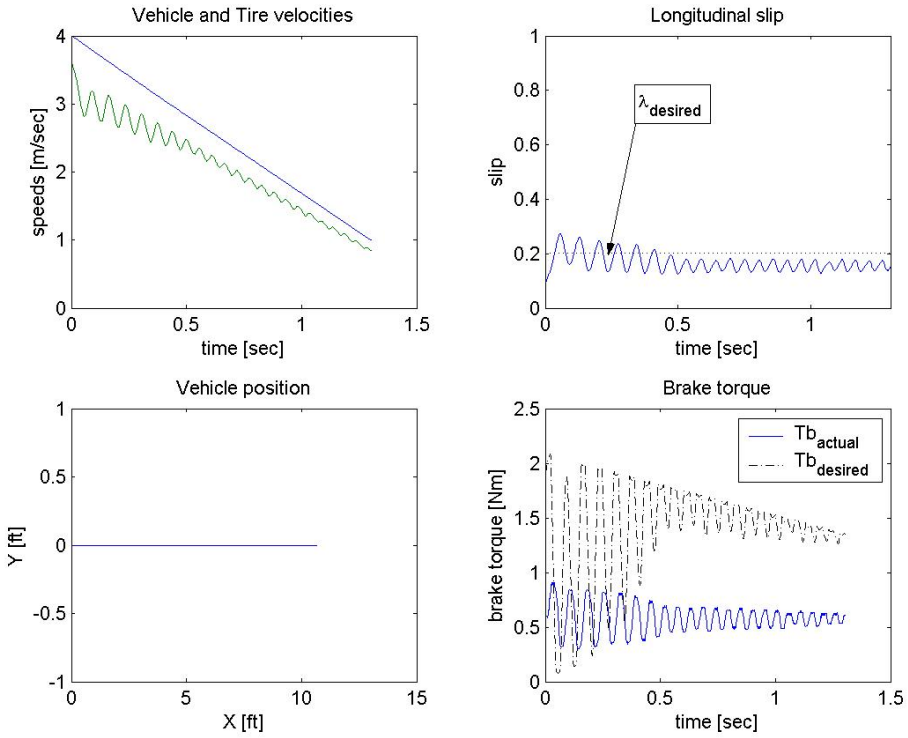


Figure 4.23: HIL test results for Straightline Braking with Sliding Mode ABS.

**HIL test results for Straightline Panic Braking with transition in the surface from a high $\mu$ to low $\mu$ value at time $T = 0.75sec$, with Sliding Mode ABS:-**

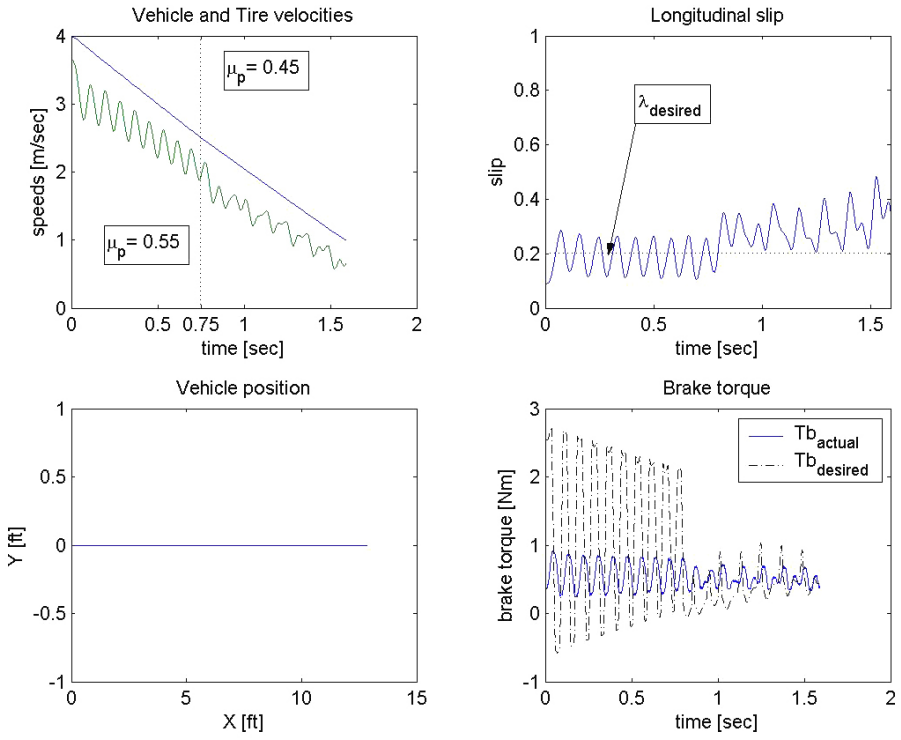


Figure 4.24: HIL test results for Braking with surface transition and Sliding Mode ABS.

**HIL test results for Panic Braking while Turning with Sliding Mode ABS:-**

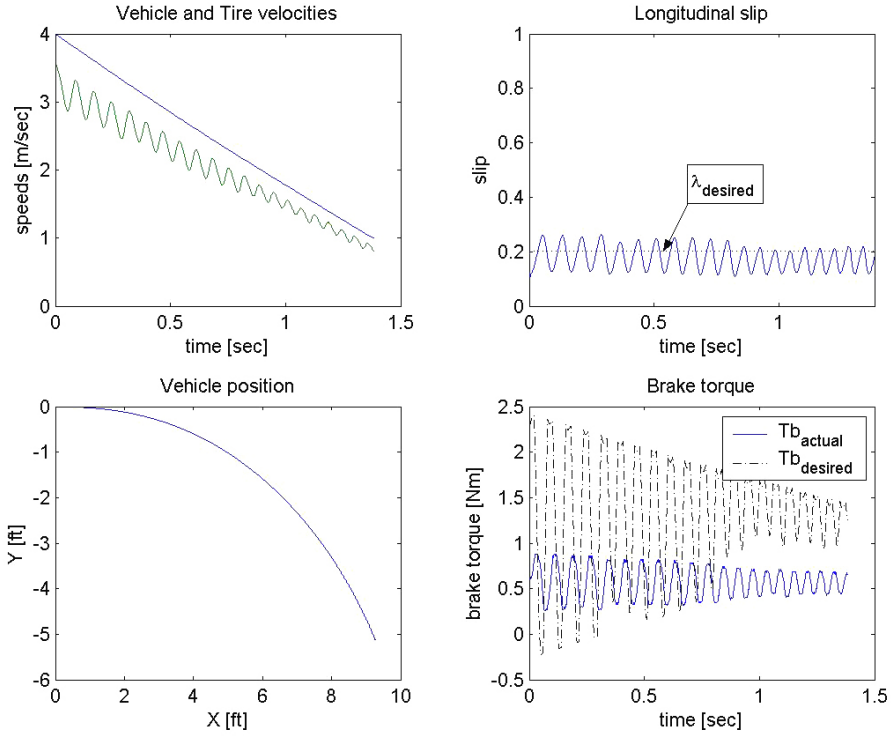


Figure 4.25: HIL test results for Braking while Turning with Sliding Mode ABS.

### 4.4.1 Results Discussion

From all the simulation and HIL testing of the brake system, with and without an ABS controller, the following observations can be made.

- The cascade control scheme works. The redesign efforts have been fruitful. The brake system working in closed loop with lead compensator certainly responds well to the control input specified by the ABS control algorithms. The cascade scheme facilitates simpler formulation and implementation for the algorithms. Although there is large steady state error the response time of the brake system is very much reduced.

- The stopping distance was reduced appreciably by employing the ABS. The vehicle maintained steering response with ABS (the vehicle negotiates the turn), while it skids off the track without ABS (see Fig. 4.10). These observations confirm that the ABS is a critical safety system in automobiles.

- Sliding mode control fares better than bang-bang control, both in simulation and test results, in terms of reducing the stopping distance. This is explained by the fact that in sliding mode control the longitudinal slip is regulated at a fixed value of $0.2 \pm 0.05$ (where $\Phi = 0.05$ is chosen for chattering reduction) which happens to coincide with the maximum traction offered by the pavement, for most surfaces. In the case of bang-bang control however, the switching is effected between slip values of $\{0.1, 0.25\}$, a range that is further expanded on account of uncertainties in the system. This implies that bang-bang control cannot deliver the best traction continuously.

It should be noted that the performance of sliding mode control degrades to that of bang-bang control if the gain of the controller is indefinitely increased. This happens because, with increase in gain the switching portion of the control, i.e., $u_s$ becomes dominant, and when the system does not respond as fast as the control demands, the control input becomes entirely switching in nature, i.e., bang-bang type.

- Bang-bang control shows an improvement in stopping distance reduction in the case of pavement transition, while the performance of sliding mode drops marginally. A change in the surface causes changes in the slip value at which the maximum traction is available. As the slip range over which bang-bang control operates is large (when compared to that of sliding mode), it could encompass this new peak friction slip value. The average friction value over the slip range will then be more (than that for sliding mode) and hence the stopping distances drop.

  In the case of sliding mode, since it is inherently robust in nature, it compensates for any changes in the pavement (and/or the system) and hence can regulate the slip at the desired value. However, if the sliding mode control was designed to 'track' a desired slip value as against regulating it at a fixed value, the problem can be overcome. All that is needed is a routine to 'estimate' the slip value at which the peak friction coefficient occurs for any pavement 'online', i.e., while in the panic braking maneuver. Then, with a slightly more complicated formulation, the sliding mode control can be made to follow the desired slip value, thereby ensuring optimum performance under any pavement.

  The development of a routine that can estimate the pavement characteristics 'online' is an area of active research. Pasterkamp and Pacejka [27]

discuss using the brush model of the tire to estimate the pavement friction. Gustafsson [28] describes an algorithm to estimate the friction value based on tire slip measurement. Kiencke [29] uses the vehicle acceleration measurements to do the same. Uchanski [30] describes using digital signal processing techniques to estimate the road friction based on only the tire speed sensors.

Another point of interest in the working of sliding mode control is that, for perfect regulation of slip, the control input, i.e., the brake torque, switches between a large positive and a large *negative* value (see Fig. 4.23). A positive torque is one which works to decelerate the tire, while a negative torque is one which accelerates it. In the event of panic braking, the reaction of the driver would be apply the brakes hard. As the brakes are passive devices (in the sense that they do not inject power into the system but only take away from it) they can only apply a positive brake torque (i.e., $\tau_{brake}$ is positive definite), which is a severe handicap for the working of the sliding mode control.

If the sliding variable is defined as $s = \lambda - \lambda_d$, then the switching control $u_s = -\eta \cdot sgn(s)$ is positive when $s$ is negative, i.e., when $\lambda < \lambda_d$ and the brake system works fine. But when $\lambda$ increases beyond $\lambda_d$ the control $u_s$ becomes negative, but the brake system can only apply zero torque (because they are passive). Thus when the sliding variable $s$ goes positive, control is lost. One of the ways to mitigate this problem is to use different bounds on $\Phi$ for positive and negative going $s$.

# Chapter 5

# Conclusion

The research work which culminated in this thesis work is summarized first. Then the essential theoretical and practical contributions made by this work are discussed.

The thesis can be summarized as below. The objective of the research work was to examine ABS control prototyping with a one-fifth scaled vehicle test-bed. The subpar performance of the brake system, as demonstrated by previous works, required its redesign. Due to the incomplete parametric data regarding the brake system, and the manifest static nonlinearities which played sigficant role in its performance, an experimental approach (frequency response testing) was adopted to model the brake sytem. The redesign efforts concentrated on mitigating the effects of the nonlinearities and improving the dynamic response of the brakes by using a phase-lead compensator. Following the redesign, a vehicle model suitable for control design was developed. Two control schemes, namely, Bang-Bang control and Sliding Mode Control, were then formulated for ABS and fine-tuned by simulations. The control algorithms were transferred from the simulation environment to the test environment using interface tools. Final control evaluation was done by performing a hardware-in-the-loop testing with the scaled vehicle setup. The improvement in stopping distance yielded by the ABS control algorithms over braking with no ABS, under panic circumstances, was used as a yardstick for com-

parison. Three commonly encountered driving scenarios, straightline braking on a single surface, with a surface transition and braking while turning, were considered and the ABS performance was shown to be satisfactory in each case. The test results are presented with a discussion.

The thesis makes two useful theoretical contributions. The first is to use the method of 'describing functions' to characterize the significant static nonlinearities in the system and derive the overall system transfer function by augmenting them with the linear system dynamics. Using the describing function approximation not only helped to explain the system behavior, but also resulted in quantitative definitions of the significant nonlinearities, which could then guide system redesign to overcome their effects. Static nonlinearities (deadzone, saturation etc.,) can have considerable impact on the system behavior in scaled systems and accounting for them sufficiently well becomes important, as demonstrated in the scaled vehicle brake system.

The second contribution is to employ a 'cascade scheme' for the ABS control. The specific nature of the disk brake systems uncouples the dynamics of the vehicle and the tire from that of the brake system. This can be successfully exploited to reduce the complexity of the ABS control schemes. The result is a modular control structure, which makes ABS controls independent of any specific brake system. Changes to the brake system can be made without having to modify the ABS controls. The cascade ABS controller scheme was shown to work effectively in regulating the tire slip value.

The most important practical result achieved in the thesis is the demonstration of the process of vehicle control prototyping using a scaled vehicle test-bed. The salient steps in control prototyping were carried out, with the process culminating in the hardware-in-the-loop testing of the designed con-

trol algorithms with the scaled vehicle setup. The process highlighted the benefits of efficient integration of simulation and testing tools. The control algorithms are then put in dimensionless form using $\pi$ parameters (see Appendix A.1.2), thereby extending it to full-sized vehicles. The other valuable practical contribution is the quantitative characterization of the scaled test vehicle (supplementing the parameters developed by Al-Sharif [1]), the tire-pavement interaction and the vehicle brake system. The results can be employed in any future investigations with the scaled vehicle test-bed.

# Appendices

# Appendix A

# System Characterization

Numerical values of the relevant parameters of the primary components of the scaled vehicle ABS test environment, i.e., the test vehicle and the brake system are listed in the following sections.

## A.1 Scaled Vehicle Parameters

Table A.1: Scaled Vehicle Parameters

| *Parameter* | *Description* | *Value* | *Units* |
|---|---|---|---|
| $M$ | Mass of the vehicle | 8.8 | $kg$ |
| $L$ | Wheel base | 0.46 | $m$ |
| $W_f$ | Weight on the front axle | 36.3 | $N$ |
| $W_r$ | Weight on the rear axle | 50.0 | $N$ |
| $L_f$ | Distance of the $C.G.$ from the front axle | 0.27 | $m$ |
| $L_r$ | Distance of the $C.G.$ from the rear axle | 0.19 | $m$ |
| $H$ | Height of the $C.G.$ from the pavement | 0.07 | $m$ |
| $J_z$ | MOI[1] of the vehicle about the $Z$-axis | 0.237 | $kg$-$m^2$ |
| $J_{tire}$ | MOI[1] of the tire about the rotational axis | $1\times10^{-3}$ | $kg$-$m^2$ |
| $R_{tire}$ | Radius of the tire | 0.061 | $m$ |
| $\delta_{max}$ | Max. steering angle (measured at the tires) | 10 | degrees |

[1]Moment of Inertia—Moment Of Inertia of the vehicle about its $Z$-axis (as per the SAE body-fixed axis system), determined from the 'bi-filar pendulum' experiment [31].

### A.1.1 $\pi$–Parameters

The '$\pi$' parameters, or the 'dimensionless numbers', of the scaled vehicle are derived in this section. By re-formulating the ABS control algorithms derived in Sec. 4.3 in terms of the $\pi$ terms, ideally, the control can be extrapolated to full-sized vehicles by simply changing the gain. The dynamic equations representing the motion of the scaled vehicle, as given by the Eq. 4.3 through Eq. 4.6 (see Sec. 4.2), will be used to guide the selection of the '$\pi$' parameters. The equations are repeated here.

$$M \cdot \dot{V}_x = -F_{xf} \cdot cos(\delta) - F_{yf} \cdot sin(\delta), \tag{A.1}$$

$$M \cdot \dot{V}_y = F_{yf} \cdot cos(\delta) + F_{yr} - F_{xf} \cdot sin(\delta) - \omega_z \cdot M \cdot V_x, \tag{A.2}$$

$$J_z \cdot \dot{\omega}_z = F_{yf} \cdot cos(\delta) \cdot L_f - F_{xf} \cdot sin(\delta) \cdot L_f - F_{yr} \cdot L_r, \tag{A.3}$$

$$J_{tire} \cdot \dot{\omega}_{tire} = F_{xf} \cdot R_{tire} - \tau_{brake}. \tag{A.4}$$

The longitudinal force on the front tires, $F_{xf}$, can be written as,

$$\begin{aligned} F_{xf} &= \mu \cdot W_f \\ &= \mu \cdot (M \cdot g) \cdot \left(\tfrac{L_r}{L}\right). \end{aligned}$$

where, $(M \cdot g) = W = W_f \cdot \left(\frac{L}{L_r}\right) = W_r \cdot \left(\frac{L}{L_f}\right)$.

Re-writing the equations A.1 and A.2 after dividing each term by $(M \cdot g)$ and substituting for $F_{xf}$,

$$\left(\frac{\dot{V}_x}{g}\right) = -\mu \cdot \left(\frac{L_r}{L}\right) \cdot cos(\delta) - \left(\frac{F_{yf}}{W_f}\right)\left(\frac{L_r}{L}\right) \cdot sin(\delta)$$

$$\left(\frac{\dot{V}_y}{g}\right) = \left(\frac{F_{yf}}{W_f}\right)\left(\frac{L_r}{L}\right) \cdot cos(\delta) + \left(\frac{F_{yr}}{W_r}\right)\left(\frac{L_f}{L}\right) - \left(\frac{L_r}{L}\right) \cdot sin(\delta) - \left(\frac{\omega_z \cdot V_x}{g}\right)$$

Re-writing the equation A.3 after multiplying each term by $L$ and dividing

each term by $(M \cdot g \cdot L_f \cdot L_r)$,

$$\left(\frac{J_z}{M \cdot L_f \cdot L_r}\right) \cdot \left(\frac{\dot{\omega}_z \cdot L}{g}\right) = \left(\frac{F_{yf}}{W_f}\right) \cdot cos(\delta) - \mu \cdot sin(\delta) - \left(\frac{F_{yr}}{W_r}\right)$$

The equation A.4, when divided by $(M \cdot g \cdot R_{tire})$, yields

$$\left(\frac{J_{tire}}{M \cdot R_{tire}^2}\right) \cdot \left(\frac{\dot{\omega}_{tire} \cdot R_{tire}}{g}\right) = \left(\frac{1}{2}\right) \cdot \mu \cdot \left(\frac{L_r}{L}\right) - \left(\frac{\tau_b}{M \cdot g \cdot R_{tire}}\right)$$

It is clear from the above four equations that the 'bracketed' terms are dimensionless, and can be regarded as the '$\pi$' parameters for the vehicle. Eleven $\pi$-terms, representing geometric, kinematic and dynamic similarities between scaled and full-sized vehicles, can be extracted from the equations and are listed in table A.2.

The $\pi$-parameters can also be derived in a more formal way by following the procedure described below [32].

1. List all the variables involved in the analysis, $V_i$, where $i = 1, 2 \ldots$ n. In the present example, these include all the variables listed in equations A.1 through A.4.

2. Identify all the fundamental dimensions required to represent the set of variables $V_i$, namely $D_j$ ($M$ass, $L$ength, $T$ime etc.), where $j = 1, 2 \ldots$r.

3. Form the matrix $E \in \Re^{n \times r}$ of the power terms of the dimensions $D_j$ in the $V_i$ dimensional equations. For example, if

   $$[V_1] = [D_1]^{p_{11}} \cdot [D_2]^{p_{12}} \cdots [D_r]^{p_{1r}}$$

   then $p_{11}$, $p_{12}$,..., $p_{1r}$, form the elements of the first row in the matrix corresponding to $V_1$.

Table A.2: $\pi$-parameters for the Scaled Vehicle

| $\pi\#$ | *Expression* | *Description* |
|---|---|---|
| $\pi_L$ | $\frac{L_f}{L_r}$ | Vehicle $C.G.$ position parameter |
| $\pi_z$ | $\frac{\omega_z \cdot V_x}{g}$ | Turn vector(expressed as a cross-product, $\overrightarrow{\omega_z} \times \frac{\overrightarrow{V_x}}{g}$) |
| $\pi_1$ | $\frac{\dot{V}_x}{g}$ | Longitudinal acceleration in 'g' units |
| $\pi_2$ | $\frac{\dot{V}_y}{g}$ | Lateral acceleration in 'g' units |
| $\pi_3$ | $\frac{\dot{\omega}_z \cdot L}{g}$ | Yaw acceleration in 'g' units |
| $\pi_4$ | $\frac{\dot{\omega}_{tire} \cdot R_{tire}}{g}$ | Tire (circumferential) acceleration in 'g' units |
| $\pi_{yf}$ | $\frac{F_{yf}}{W_f}$ | Front tire cornering coefficient (see [21] for definition) |
| $\pi_{yr}$ | $\frac{F_{yr}}{W_r}$ | Rear tire cornering coefficient |
| $\pi_\mu$ | $\mu$ | Tire-ground friction coefficient |
| $\pi_{Jz}$ | $\frac{J_z}{M \cdot L_f \cdot L_r}$ | Z-axis rotational inertia factor |
| $\pi_{Jt}$ | $\frac{J_{tire}}{M \cdot R_{tire}^2}$ | Tire-vehicle comparative inertia |
| $\pi_\tau$ | $\frac{\tau_b}{M \cdot g \cdot R_{tire}}$ | Dimensionless control input |

$$E_{n\times r} = \begin{array}{c} \\ V_1 \\ \vdots \\ V_n \end{array} \begin{array}{c} \begin{array}{cccc} D_1 & D_2 & \dots & D_r \end{array} \\ \begin{pmatrix} p_{11} & p_{12} & \dots & p_{1r} \\ \vdots & \vdots & \ddots & \vdots \\ p_{n1} & p_{n2} & \dots & p_{nr} \end{pmatrix} \end{array}$$

4. Divide the matrix $E$ is into two sub-matrices $E_A \in \Re^{r\times r}$ and $E_B \in \Re^{(n-r)\times r}$ such that $E_A$ is not *singular*, i.e., $\text{rank}(E_A) = r$. This is equivalent to finding $r$ variables among $V_i$ which do not form a dimensionless group amongst themselves. The number of dimensionless groups that can be formed is then equal to $m = n - r$.

$$E_{n\times r} \;=\; \left(\begin{array}{c} E_A \in \Re^{r\times r} \\ \hline E_B \in \Re^{m\times r} \end{array}\right)$$

5. Form a matrix $F \in \Re^{n\times m}$ as,

$$F_{n\times m} \;=\; \left(\begin{array}{c} E_C \in \Re^{r\times m} \\ \hline I \in \Re^{m\times m} \end{array}\right)$$

where, $E_C$ is given by $E_C = -\left[E_B \times (E_A)^{-1}\right]^T$. The two matrices $E$ and $F$ are written in augmented form as an $n \times n$ matrix as shown below. The columns of the matrix $F$ then represent the equations of the dimensionless groups or $\pi$-parameters in terms of the variables set $V_i$.

| | $D_1$ $\cdots$ $D_r$ | $\pi_1$ $\cdots$ $\pi_m$ |
|---|---|---|
| $V_1$ <br> $\vdots$ <br> $V_r$ | $\mathbf{E_A}$ | $\mathbf{E_C}$ |
| $V_{r+1}$ <br> $\vdots$ <br> $V_n$ | $\mathbf{E_B}$ | $\mathbf{I}$ |

For the scaled vehicle system, the augmented matrix to determine the $\pi$-parameters is shown below.

| | $M$ | $L$ | $T$ | $\pi_1$ | $\pi_2$ | $\pi_3$ | $\pi_4$ | $\pi_5$ | $\pi_6$ | $\pi_7$ | $\pi_8$ | $\pi_9$ | $\pi_{10}$ | $\pi_{11}$ |
|---|---|---|---|---|---|---|---|---|---|---|---|---|---|---|
| $L_r$ | 0 | 1 | 0 | 0 | 0 | 0 | -2 | -2 | -1 | -1 | 0 | 0 | 0 | 0 |
| $g$ | 0 | 1 | -2 | -1 | -1 | -1 | 0 | 0 | 0 | 0 | -1 | -1 | -1 | -1 |
| $M$ | 1 | 0 | 0 | -1 | -1 | -1 | -1 | -1 | 0 | 0 | 0 | 0 | 0 | 0 |
| $F_{xf}$ | 1 | 1 | -2 | 1 | 0 | 0 | 0 | 0 | 0 | 0 | 0 | 0 | 0 | 0 |
| $F_{yf}$ | 1 | 1 | -2 | 0 | 1 | 0 | 0 | 0 | 0 | 0 | 0 | 0 | 0 | 0 |
| $F_{yr}$ | 1 | 1 | -2 | 0 | 0 | 1 | 0 | 0 | 0 | 0 | 0 | 0 | 0 | 0 |
| $J_z$ | 1 | 2 | 0 | 0 | 0 | 0 | 1 | 0 | 0 | 0 | 0 | 0 | 0 | 0 |
| $J_{tire}$ | 1 | 2 | 0 | 0 | 0 | 0 | 0 | 1 | 0 | 0 | 0 | 0 | 0 | 0 |
| $L_f$ | 0 | 1 | 0 | 0 | 0 | 0 | 0 | 0 | 1 | 0 | 0 | 0 | 0 | 0 |
| $R_t$ | 0 | 1 | 0 | 0 | 0 | 0 | 0 | 0 | 0 | 1 | 0 | 0 | 0 | 0 |
| $\dot{V}_x$ | 0 | 1 | -2 | 0 | 0 | 0 | 0 | 0 | 0 | 0 | 1 | 0 | 0 | 0 |
| $\dot{V}_y$ | 0 | 1 | -2 | 0 | 0 | 0 | 0 | 0 | 0 | 0 | 0 | 1 | 0 | 0 |
| $\dot{\omega_z}$ | 0 | 1 | -2 | 0 | 0 | 0 | 0 | 0 | 0 | 0 | 0 | 0 | 1 | 0 |
| $\dot{\omega_{tire}}$ | 0 | 1 | -2 | 0 | 0 | 0 | 0 | 0 | 0 | 0 | 0 | 0 | 0 | 1 |

From the augmented matrix, the $\pi$ terms are extracted by writing, say $\pi_1$, as

$$\pi_1 \quad = \quad [g]^{-1} \cdot [M]^{-1} \cdot [F_{xf}]^1 \quad = \quad \frac{F_{xf}}{M \cdot g}$$

All the other $\pi$ terms can be similarly determined and it can be seen that they are identical to those obtained in the table A.2.

### A.1.2 Dimensionless Forms of ABS Controllers

With the knowledge of the $\pi$ parameters, the ABS controller can be reformulated in dimensionless form as below.

#### Dimensionless Form of Bang-Bang ABS Controller

As the bang-bang controller works based on the longitudinal slip value (which is dimensionless in itself), the controller can be extrapolated to the full-sized vehicles directly. The value of the maximum brake torque to be applied however depends upon the particular vehicle construction.

**Dimensionless Form of Sliding Mode ABS Controller**

The Eq. 4.10, representing the vehicle model, was used to formulate the sliding mode ABS controller and are repeated here.

$$\begin{aligned} M \cdot \dot{V}_x &= -W_f \cdot \mu \\ J_{tire} \cdot \dot{\omega}_{tire} &= \left(\frac{1}{2}\right) \cdot W_f \cdot \mu \cdot R_{tire} - \tau_{brake} \\ \lambda &= \left(1 - \frac{\omega_{tire} \cdot R_{tire}}{V_x}\right) \end{aligned}$$

They can be re-written in terms of the $\pi$ terms derived above as,

$$\begin{aligned} \dot{\pi}_1 &= -\pi_\mu \cdot \pi_L \\ \pi_{Jt} \cdot \dot{\pi}_4 &= \frac{1}{2} \cdot \pi_\mu \cdot \pi_L - \pi_\tau \\ y(=\lambda) &= 1 - \left(\frac{\pi_4}{\pi_1}\right) \end{aligned}$$

Following the procedure outlined in Sec. 4.3.2, the sliding variable is defined as $s = y - y_d$, so that

$$\begin{aligned} \dot{s} &= \dot{y} \\ &= \frac{\dot{\pi_1}(1-\lambda) - \dot{\pi_4}}{\pi_1} \end{aligned}$$

Again, by having $\dot{s} = -\eta \cdot sgn(s)$, the control input in dimensionless form can be written by simplifying the above equation as,

$$\pi_\tau = \pi_\mu \cdot \pi_L \cdot \pi_{Jt}(1-\lambda) + \frac{1}{2} \cdot \pi_\mu \cdot \pi_L - \pi_1 \cdot \pi_{Jt} \cdot \eta \cdot sgn(s)$$

It should be noted that the above equation reverts to Eq. 4.18, when all the $\pi$ terms are substituted from the table A.2.

The value of the controller gain, $\eta$, will need to be determined from the numerical values of the $\pi$ parameter, and hence will be different for scaled

and full-sized vehicles. But the control structure remains the same. This is under the assumption that the full-sized vehicle will be represented by the same simple vehicle model (derived in Sec. 4.2).

## A.2 Brake System Parameters

The bond graph representation of the brake system is shown in Fig. 3.5. The parameters of the three subsystems, the motor, the transmission mechanism and the disk-caliper mechanism are listed here. The experimental procedure for determining some of the parameters are outlined.

### Servo Motor

Table A.3: Servo Motor Parameters

| *Parameter* | *Description* | *Value* | *Units* |
|---|---|---|---|
| $K_m$ | Motor torque constant | 0.882 | $Nm/A$ |
| $R_m$ | Motor resistance | 7.1 | $\Omega$ |
| $J_m$ | Motor inertia | $4.15 \times 10^{-4}$ | $kg\text{-}m^2$ |

The motor torque constant is determined by applying known voltage values to the motor at no load and measuring the output speed. The linear trend is obtained by plotting the speed along $Y$-axis and voltage along $X$-axis. The slope of the line yields the motor torque constant. The plot of the speed versus the voltage applied for the motor is shown in Fig. A.1.

The variation of the motor damping characteristics with the motor speed is also determined from the above analysis. The current to drive the motor, under no-load condition, at different speeds was measured. Under no-load condition, the input power is entirely dissipated in the motor resistance and

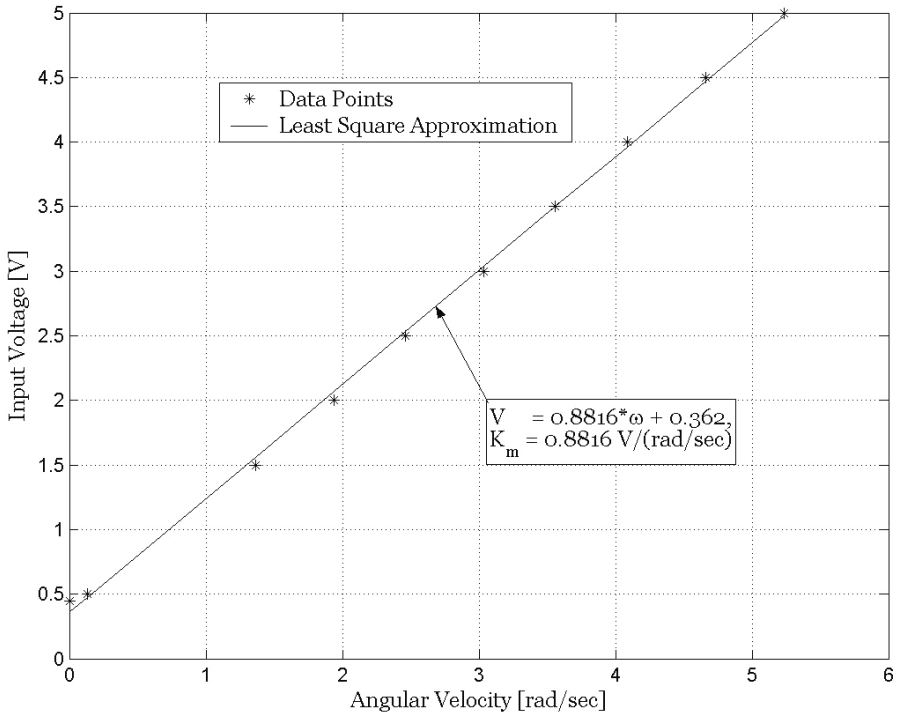


Figure A.1: Motor torque constant determination.

mechanical damping. With the knowledge of the motor torque constant, the torque required to overcome the damping is calculated as the product of the current and the torque constant. Fig. A.2 shows the plot of the damping torque versus the motor speed. It is clear that the motor exhibits stiction which introduce a deadzone effect in the motor response.

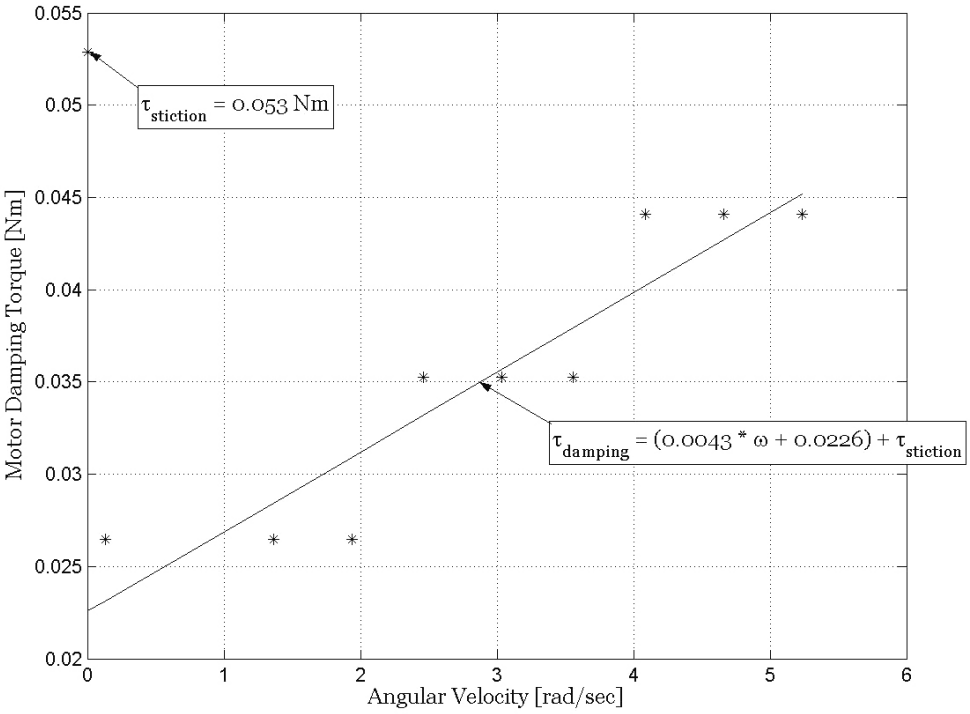


Figure A.2: Motor damping characteristics.

Table A.4: Force Transmission Mechanism Parameters

| *Parameter* | *Description* | *Value* | *Units* |
|---|---|---|---|
| $R_{arm}$ | Motor torque arm length | 18 | $mm$ |
| L | Lever length | 30 | $mm$ |
| $R_{cam}$ | Effective cam radius | 5.5 | $mm$ |
| $M_{cable}$ | Mass of the cable | $2\times10^{-3}$ | $kg$ |
| $J_{cam}$ | Moment of inertia of the lever-cam about the axis of rotation | $0.33\times10^{-6}$ | $kg\text{-}m^2$ |

### Disk-Caliper Mechanism

The effective radius of the brake disk = 0.025 mm.

The coefficient of friction between the brake disk and the calipers is determined by applying a known normal force to the brake pads and measuring the torque that needs to be applied to the disk to initiate rotation (i.e., to break the equilibrium). The tangential force is determined from the torque. The plot of the tangential force versus the normal force is shown in Fig. A.3. The slope of the linear trendline represents the friction coefficient.

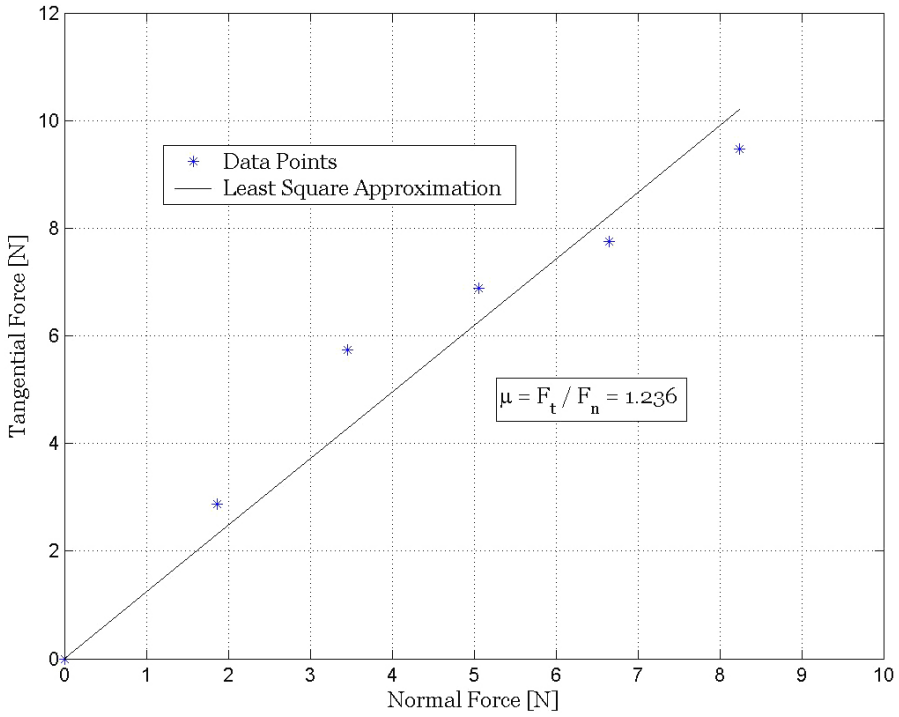


Figure A.3: Brake caliper-disk friction coefficient.

# Appendix B

# ABS Test Procedure using Scaled Vehicle Setup

A detailed description the scaled vehicle testing procedure can be found in Al-Sharif [1], pp.73–74. A brief outline is presented here.

- **Preparations:-**

  The LabVIEW VI along with any *DLL*s which will be used for testing and data collection are downloaded onto the remote Real-time PXI engine via TCP/IP (into the directory "C:/NI-RT/Startup/"). A host VI is set up to communicate with the remote VI over the VI Server so as to retrieve the data collected during the test from the PXI engine into the host PC.

  The test vehicle is hitched to the DAQ cards via the umbilical cord and the power supply to the DC motor driver amplifiers and all the sensors on-board the test vehicle is turned on.

- **Testing:-**

  The test vehicle is pulled up on the ramp using the winch motor (which is mounted at the top of the ramp), to a pre-determined height $H$. The ramp merges with the track in a smooth circular arc (radius = 1.78 m), which results in the test vehicle velocity increasing as $V \propto g \cdot sin(\theta)$ for

$0 \leq \theta \leq \frac{\pi}{2}$ with time, as shown in Fig. B.1. The ramp exit velocity (the initial velocity for the test) is roughly equal to $\sqrt{2 \cdot g \cdot H}$ where $H$ is the height of the vehicle $C.G.$ from the ground. As seen in the figure, the transition of the test vehicle velocity from the acceleration phase to the deceleration phase (during the braking maneuver) occurs smoothly enough to assume that the initial conditions for the ABS tests can be obtained repeatably.

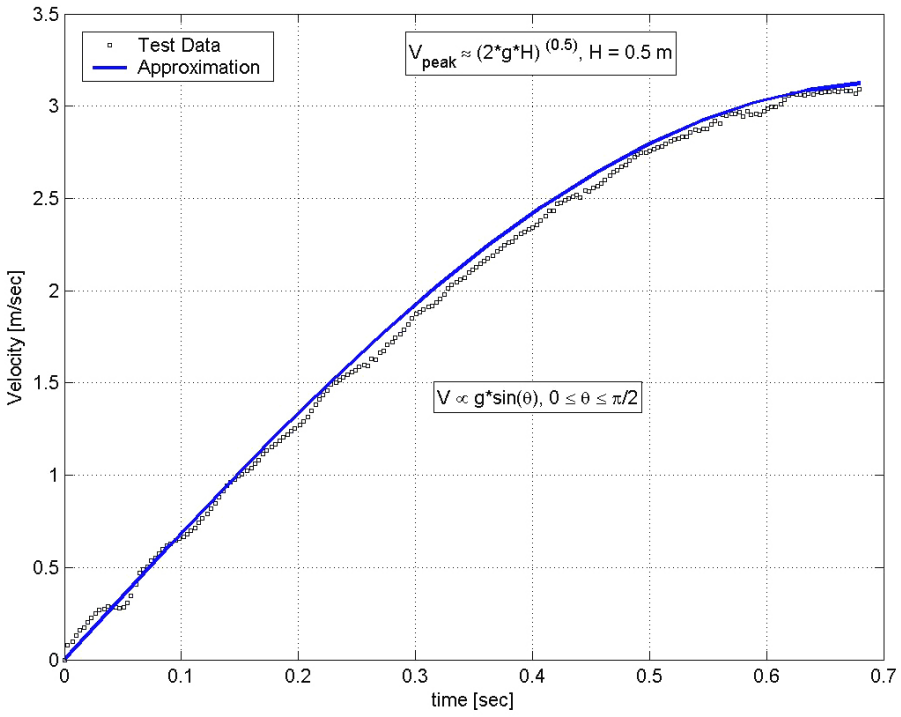


Figure B.1: Test Vehicle velocity on the accelerating ramp.

The test surface is spread onto the track. Crash guards are placed surrounding the track to prevent the vehicle from veering out of the track

(due to disturbances).

The vehicle release is achieved by operating a servo motor on the test vehicle which is programmed in the VI. The braking is initiated at a fixed time of $0.85sec$ after the release for every test. The value of the braking initiation time has been determined experimentally to coincide with the time the vehicle velocity has steadied after leaving the ramp.

Once the braking maneuver is complete and the data collection has stopped, the power supply is turned off (to prevent overheating of the motor driver amplifiers).

- Data Analysis:-

  Following the test, the data is retrieved from the remote PXI engine onto the host PC for data analysis.

# Bibliography


[1] Amrou Adly Al-Sharif, *Design and Development of a Scaled Test Laboratory for the study of ABS and other Active Vehicle Control Systems*, Thesis, The University of Texas at Austin, August, 2002.

[2] Anish Mathews, *Rule-based fuzzy logic control of ABS with a one-fifth scale test vehicle*, Thesis, The University of Texas at Austin, December 2002.

[3] *Brake Systems for Passenger Cars*, Robert Bosch GmbH, 1994.

[4] B. T. Kulakowski, M. Chi, C. Lin, *Measurement and Modeling of Truck Tire Traction Characteristics*, Vehicle Tire-Pavement Interface, ASTM STP 1164, 1992, pp.112–124.

[5] Fangjun Jiang, *An application of nonlinear PID control to a class of Truck ABS problems*, Proceedings of the $40^{th}$ IEEE Conference on Decision and Control, December 2001.

[6] Cem Ünsal, Pushkin Kachroo, *Sliding Mode Measurement Feedback Control for Antilock Braking Systems*, IEEE Transactions on Control Systems Technology, Vol.7, No. 2, March 1999.

[7] Will, A.B., Hui, S. and Żak, S.H. (1998) *Sliding mode wheel slip controller for an Antilock Braking System*, Int. J. of Vehicle Design, Vol. 19, No. 4, pp.523–539.

[8] Seongho Choi and Dong-Woo Cho, *Design of Nonlinear Slidng Mode controller with Pulse Width Modulation for Vehicular Slip Ratio Control*, Vehicle System Dynamics, 2001, Vol. 36, No. 1, pp.57–72.

[9] Marjan Voit, Yann Chamaillard and Grard Lon Gissinger, *Methodology for the Design of a New Strategy in Vehicle Braking: Simulation and Comparison of Algorithms*, JSAE Review, Volume 16, Issue 2, April 1995, pp.220-221.

[10] Yonggon Lee, Stanislaw H. Zák, *Designing a genetic Neural Fuzzy Antilock-Brake-System controller*, IEEE Transactions on Evolutionary Computation 6(2): pp.198–211, 2002.

[11] Ralf Klein, Herbert Eichfeld, *Antilock-Braking System and Vehicle Speed Estimation using Fuzzy Logic*, $1^{st}$ Embedded Computing Conference, October 1996.

[12] Garrick Forkenbrock, Mark Flick, W. Riley Garrott, *A Comprehensive Light Vehicle Antilock Brake System Test Track Performance Evaluation*, Society of Automotive Engineers, 1998.

[13] Sean Brennan, Andrew Alleyne, *Robust Scalable Vehicle Control via Non-dimensional Vehicle dynamics*, Vehicle System Dynamics, 2001, Vol. 36. No. 4–5, pp.255–277.

[14] J. Sika, J. Hilgert, Dr. T. Bertram, Prof. J. P. Pauwelussen, Prof. M. Hiller, *Test facility for lateral control of a Scaled Vehicle in an Automated Highway System*, University of Delft,Gerhard-Mercator-University.

[15] Pushkin Kachroo and Kaan Özbay, *Microprocessor Controlled Small Scale Vehicles for Experiments in Automated Highway Systems*, The Korean Transport Policy Review, Vol. 4, No. 3, pp. 145-178, 1997.

[16] Jerry Ferdinand Cuderman II, *Performance of Passenger Vehicle Anti-Lock Braking Systems: An Experimental Study*, Dissertation, The University of Texas at Austin, December, 2001.

[17] Katsuhiko Ogata, *Modern Control Engineering*, $2^{nd}$ Ed., Englewood Cliffs, N.J. Prentice Hall, 1990.

[18] Michael Hafner, Oliver Jost, Rolf Isermann, *Mechatronic Design approach for Engine Management Systems*, Mechatronics, Volume 12, Issue 8, October 2002, pp.1035-1046.

[19] FGModellsport, *FGModellsport Catalog 2000*, RC World and RC Publishers, July, 2000.

[20] A. K. Baker, *Vehicle Braking*, London: Pentech, 1986.

[21] J. Y. Wong, *Theory of Ground Vehicles*, New York: John Wiley & Sons, 1993.

[22] Crash Avoidance Research, NHTSA Vehicle Research and Test Center, Ohio.

[23] Thomas D. Gillespie, *Fundamentals of Vehicle Dynamics*, Society of Automotive Engineers, Inc., 1992.

[24] Dean C. Karnopp, Donald L. Margolis, Ronald C. Rosenberg, *System Dynamics: A Unified Approach*, Second Ed., John Wiley & Sons, Inc., 1990.

[25] J.-J. E. Slotine, W. Li, *Applied Nonlinear Control*, Englewood Cliffs, N., 1991.

[26] Wilfrid Perruquetti, Jean Pierre Barbot, *Sliding Mode Control in Engineering*, Marcel Dekker Inc., 2002.

[27] W. R. Pasterkamp, H. B. Pacejka, *The tyre as a sensor to estimate friction*, Vehicle System Dynamics, Vol. 27 (1997), pp. 409–422.

[28] Fredrik Gustafsson, *Slip-based Tire-Road Friction Estimation*, Automatica, Vol. 33, No. 6, pp. 1087–1099, 1997.

[29] U. Kiencke, A. Daiß, *Estimation of tire friction for enhanced ABS-Systems*, Internatinoal Symposium on Advanced Vehicle Control, pp. 515–520, 1994.

[30] Michael R. Uchanski, *Road friction estimation for automobiles using Digital Signal Processing Methods*, Dissertation, University of California, Berkeley, 2001.

[31] Robert F. Steidel, Jr., *An Introduction to Mechanical Vibrations*, 3rd ed. Wiley, c1989.

[32] Robert W. Fox, Alan T. McDonald, *Introduction to Fluid Mechanics*, 5th ed., J. Wiley, 1998.

# Vita

Chinmaya Baburao Patil was born on September 7, 1978, in Hubli, India, as the second son of Baburao Rangarao Patil and Leela Baburao Patil. He completed lower division education in Bangalore and Hubli, and high school in Belgaum. He then enrolled in the Karnataka Regional Engineering College (now, National Institute of Technology), Surathkal, India, for undergraduate education in Mechanical Engineering, in 1996. He graduated in 2000, receiving a Gold Medal from the Mangalore University in the discipline of Mechanical Engineering. During the following year, he was employed as a Design Engineer with Tata AutoComp Ltd., Pune. In Fall 2001, he entered The University of Texas at Austin to pursue graduate studies in Mechanical Engineering, with a scholarship to study abroad from the distinguished J. N. Tata Endowment Trust. Starting Summer, 2002, he has been working as a research assistant under the supervision of Dr. R. G. Longoria. The research work, funded by National Instruments, resulted in two publications, a journal paper for the International Journal of Vehicle Autonomous Systems (to appear) and a paper for the $42^{nd}$ IEEE Conference on Decision and Control, besides the Master's thesis.

Permanent address: "Omkar", MIG–12, #102, Akshaya Park,
Gokul Road, Hubli 580030
India.

This thesis was typeset with LaTeX[†] by the author.

[†]LaTeX is a document preparation system developed by Leslie Lamport as a special version of Donald Knuth's TeX Program.